Atmos. Chem. Phys. Discuss., 15, 2197–2246, 2015
www.atmos-chem-phys-discuss.net/15/2197/2015/
doi:10.5194/acpd-15-2197-2015

Atmospheric Chemistry and Physics Discussions

Uncertainties in isoprene photochemistry and emissions: implications for the oxidative capacity of past and present atmospheres and for trends in climate forcing agents

P. Achakulwisut[1], L. J. Mickley[2], L. T. Murray[3,4], A. P. K. Tai[5], J. O. Kaplan[6], and B. Alexander[7]

[1]Department of Earth and Planetary Sciences, Harvard University, Cambridge, MA, USA
[2]School of Engineering and Applied Sciences, Harvard University, Cambridge, MA, USA
[3]NASA Goddard Institute for Space Studies, New York, NY, USA
[4]Lamont-Doherty Earth Observatory, Columbia University, Palisades, NY, USA
[5]Earth System Science Programme, The Chinese University of Hong Kong, Hong Kong, China
[6]ARVE Group, Ecole Polytechnique Fédérale de Lausanne, Lausanne, Switzerland
[7]Department of Atmospheric Sciences, University of Washington, Seattle, WA, USA

Received: 29 December 2014 – Accepted: 6 January 2015 – Published: 23 January 2015

Correspondence to: P. Achakulwisut (pachakulwisut@fas.harvard.edu)

Published by Copernicus Publications on behalf of the European Geosciences Union.

ACPD
15, 2197–2246, 2015

Abstract

Current understanding of the factors controlling biogenic isoprene emissions and of the fate of isoprene oxidation products in the atmosphere has been evolving rapidly. We use a climate-biosphere-chemistry modeling framework to evaluate the sensitivity of estimates of the tropospheric oxidative capacity to uncertainties in isoprene emissions and photochemistry. Our work focuses on trends across two time horizons: from the Last Glacial Maximum (LGM, 21 000 years BP) to the preindustrial (1770s); and from the preindustrial to the present day (1990s). We find that different oxidants have different sensitivities to the uncertainties tested in this study, with OH being the most sensitive: changes in the global mean OH levels for the LGM-to-preindustrial transition range between −29 and +7 %, and those for the preindustrial-to-present day transition range between −8 and +17 %, across our simulations. Our results suggest that the observed glacial-interglacial variability in atmospheric methane concentrations is predominantly driven by changes in methane sources as opposed to changes in OH, the primary methane sink. However, the magnitudes of change are subject to uncertainties in the past isoprene global burdens, as are estimates of the change in the global burden of secondary organic aerosol (SOA) relative to the preindustrial. We show that the linear relationship between tropospheric mean OH and tropospheric mean ozone photolysis rates, water vapor, and total emissions of NO_x and reactive carbon – first reported in Murray et al. (2014) – does not hold across all periods with the new isoprene photochemistry mechanism. Our results demonstrate that inadequacies in our understanding of present-day OH and its controlling factors must be addressed in order to improve model estimates of the oxidative capacity of past and present atmospheres.

ACPD
15, 2197–2246, 2015

1 Introduction

A key player in the coupling between climate change and atmospheric chemical composition is the oxidative capacity of the troposphere, primarily characterized by the burden of the four most abundant and reactive oxidants: OH, ozone, H_2O_2, and NO_3. Estimates of the oxidative capacity of past atmospheres remain uncertain due to the limited number of historical and paleo-observations, which hinders our ability to understand the chemical, climatic, and ecological consequences of past changes in the oxidative capacity. Multiple factors govern the abundance of tropospheric oxidants, including emissions of reactive volatile organic compounds (VOCs). Isoprene (2-methyl-1,3-butadiene, C_5H_8), primarily emitted by plants, is the most abundant VOC in the present-day atmosphere after methane (Pike and Young, 2009). Recent studies have suggested the need to revise our understanding of the environmental factors controlling biogenic isoprene emissions and of its atmospheric photo-oxidation mechanism (e.g., Paulot et al., 2009a, b; Possell and Hewitt, 2011). These advances call into question the validity of existing model estimates of the oxidative capacity of past atmospheres. In this study, we use a climate-biosphere-chemistry modeling framework (Murray et al., 2014) to explore the sensitivity of the simulated oxidative capacity to uncertainties in isoprene emissions and photochemistry, and the implications for radiative forcing on preindustrial-present and on glacial-interglacial timescales. To our knowledge, this study is the first systematic evaluation of the effects of these recent developments on model estimates of the chemical composition of past atmospheres.

The atmospheric oxidative capacity determines the lifetime of many trace gases important to climate, chemistry, and human health (e.g., Isaksen and Dalsøren, 2011; Fiore et al., 2012). It may also induce oxidative stress or alter the deposition of oxidized nutrients to terrestrial and marine ecosystem (Sitch et al., 2007; Paulot et al., 2013). Furthermore, oxidants modify the radiative effects of aerosols by influencing their evolution, lifetime, and physical properties (Sofen et al., 2011). However, due to the high reactivity of most atmospheric oxidants, direct measurement of their abundance is nearly

ACPD
15, 2197–2246, 2015

impossible for the past. Late 19th-century surface ozone measurements exist but their accuracy has been debated (Pavelin et al., 1999). Atmospheric oxidants, except for H_2O_2, are not directly preserved in the ice-core record, but post-depositional processes impede quantitative interpretation of the H_2O_2 record (Hutterli et al., 2002). As summarized in Murray et al. (2014), Table 1, prior modeling studies that investigated past changes in the abundance of tropospheric oxidants disagree on the magnitude and even the sign of change. Such discrepancies call into question our ability to quantify the relative roles of sources and sinks in driving past variations in atmospheric methane concentration. Previous studies attributed these variations to changes in wetland emissions, the dominant natural source of methane to the atmosphere (e.g., Khalil and Rasmussen, 1987; Brook et al., 2000). However, more recent modeling studies suggested that potential variations in OH – the primary sink for methane – may be larger than previously thought, driven by changes in biogenic VOC emissions (e.g., Kaplan, 2002; Valdes, 2005; Harder et al., 2007).

Tropospheric oxidants are strongly coupled through atmospheric photochemical reactions, and their abundance responds to meteorological conditions, changes in surface and stratospheric boundary conditions, and changes in emissions of key chemical species such as reactive nitrogen oxides (NO_x = NO + NO_2) and VOCs. Present-day natural emissions of VOCs, which far exceed those from anthropogenic sources on a global scale, are dominated by plant isoprene emissions, which have an estimated global source ranging from approximately 500 to 750 Tg yr^{-1} (Lathière et al., 2005; Guenther et al., 2006). This large emission burden is accompanied by high reactivity; isoprene has an atmospheric chemical lifetime on the order of minutes to hours (Pike and Young, 2009). Isoprene and its oxidation products react with OH, ozone, and the nitrate radical, and are thus major players in the oxidative chemistry of the troposphere (Beerling et al., 2007). The oxidation products of isoprene also substantially contribute to secondary organic aerosol (SOA) formation (Henze and Seinfeld, 2006). Biogenic SOA, like other aerosols, affects climate by scattering and absorbing solar radiation, and by altering the properties and lifetimes of clouds (Scott et al., 2014). Un-

ACPD
15, 2197–2246, 2015

certainties in the preindustrial-to-present day changes in biogenic SOA burdens lead to large uncertainties in the anthropogenic direct and indirect radiative forcing estimates (e.g., Scott et al., 2014; Unger, 2014). Results from the Atmospheric Chemistry and Climate Model Intercomparison Project (ACCMIP) demonstrate that uncertainties remain in our understanding of the long-term trends in OH and methane lifetime, and that these uncertainties primarily stem from a lack of adequate constraints on natural precursor emissions and on the chemical mechanisms in the current generation of chemistry-climate models (Naik et al., 2013). Recent field and laboratory findings have called into question prior estimates of global burdens of isoprene for the past and future atmospheres, and have revealed new details of the isoprene photo-oxidation mechanism. First, isoprene emission from plants is well known to be strongly dependent on plant species and, for a given species, on environmental factors including temperature, light availability, and leaf age (Guenther et al., 2012). However, recent empirical studies have shown that isoprene emission by several plant taxa is also inversely correlated with atmospheric CO_2 levels, but this relationship is not yet well-constrained (e.g., Wilkinson et al., 2009; Possell and Hewitt, 2011). The biochemical mechanism for this effect remains unresolved, but evidence suggests that CO_2 concentration plays a role in partitioning carbon-substrate availability between the chloroplast and cytosol of a plant cell, and in mobilizing stored carbon sources (Trowbridge et al., 2012). Such bio-mechanisms involving a CO_2-dependence of isoprene emissions may have evolved in plants long ago.

Second, recent field studies in major isoprene-emitting regions, such as the Amazon forest (Lelieveld et al., 2008), South East Asia (Hewitt et al., 2010), and China (Hofzumahaus et al., 2009), reported large discrepancies between measured and modeled HO_x (OH + HO_2) concentrations, suggesting that VOC oxidation under low-NO_x conditions may recycle OH more efficiently than previously understood. These findings motivated numerous theoretical and experimental studies, which in turn led to extensive updates in the gas-phase isoprene photo-oxidation mechanism, in which there is greater regeneration and recycling of HO_x and NO_x under high-NO_x conditions, and of

ACPD
15, 2197–2246, 2015

HO_x under low-NO_x conditions (e.g., Paulot et al., 2009a, b). In general, greater OH-recycling enhances the efficiency of atmospheric oxidation, while greater NO_x-recycling enhances the efficiency of ozone production. However, the improved mechanism is still unable to fully reconcile measured and modeled OH concentrations (Mao et al., 2012). Moreover, global and regional modeling studies indicate that the heterogeneous HO_2 uptake by aerosols presents a potentially important HO_x sink. There remains, however, considerable uncertainty in the magnitude of this sink and its impact on tropospheric chemistry (Thornton et al., 2008) Mao et al. (2013a) proposed a new scheme in which HO_2uptake by aerosols leads to H_2O rather than H_2O_2 formation, via coupling of Cu(I) / Cu(II) and Fe(II) / Fe(III) ions. Since H_2O_2 can be readily photolyzed to regenerate OH, this new mechanism provides a more efficient HO_x removal pathway.

In support of the ICE age Chemistry And Proxies (ICECAP) project, Murray et al. (2014) developed a new climate-biosphere-chemistry modeling framework for simulating the chemical composition of the present and past tropospheres, focusing on preindustrial-to-present and glacial-interglacial transitions. The Last Glacial Maximum (LGM, ~ 19–23 kyr) spans the coldest interval of the last glacial period (~ 11.5–110 kyr) and is relatively well recorded in ice-core and sediment records, making the LGM-to-preindustrial transition a convenient glacial-interglacial analogue. Disparities in existing model studies of past tropospheric oxidant levels are partly due to differences in the model components of the Earth system allowed to vary with climate, and the differing degrees of complexity in the representation of those components (Murray et al., 2014). The ICECAP project is the first 3-D model framework to consider the full suite of key factors controlling the oxidative capacity of the troposphere at and since the LGM, including the effect of changes in the stratospheric column ozone on tropospheric photolysis rates. Murray et al. (2014) found that: (1) the oxidative capacities of the preindustrial and LGM atmospheres were both lower than that of the present day; (2) tropospheric mean OH levels appear to be well buffered in the LGM-to-preindustrial transition – a result at odds with most prior studies; (3) past changes in atmospheric methane concentrations were predominantly source-driven; and (4) the key parameters controlling

ACPD
15, 2197–2246, 2015

the oxidative capacity over LGM-present day timescales are tropospheric mean ozone photolysis rates, water vapor abundance, and total emissions of NO_x and reactive carbon.

In light of recent developments in our understanding of the isoprene photo-oxidation mechanism and of the sensitivity of plant isoprene emissions to atmospheric CO_2 levels, we build on the model study by Murray et al. (2014) to explore the sensitivity of the simulated tropospheric oxidative capacity at and since the LGM, and the ramifications for our understanding of the factors controlling the oxidative capacity. We also discuss the implications for trends in short-lived climate forcers and for interpreting the ice-core methane record. To our knowledge, this is the first model study to consider, in a systematic manner, the effect of all of the above developments on the chemical composition of the troposphere over the last glacial-interglacial time interval and the industrial era.

2 Method: model framework, model developments, and project description

2.1 The ICECAP model framework

Figure 1 illustrates the stepwise, offline-coupled climate-biosphere-chemistry model framework of the ICECAP project. This setup relies on four global models. GEOS-Chem is a global 3-D chemical transport model (CTM) with a long history in simulating present-day tropospheric ozone-NO_x-CO-VOC-BrO_x-aerosol chemistry (http://www.geos-chem.org; Bey et al., 2001; Park, 2004; Parrella et al., 2012), and includes online linearized stratospheric chemistry (McLinden et al., 2000). We use version 9-01-03 with modifications as described in Murray et al. (2014) and below. ICECAP is driven by meteorological fields from ModelE, a climate model developed at the NASA Goddard Institute of Space Studies (GISS). ModelE and related models at GISS have been used extensively in paleo-climate studies (e.g., LeGrande et al., 2006; Rind et al., 2001, 2009). Here we use the ModelE version with a horizontal resolution of 4°

ACPD
15, 2197–2246, 2015

latitude by 5° longitude, and 23 vertical layers extending from the surface to 0.002 hPa in the atmosphere. Climate in ModelE is forced by prescribed greenhouse gas levels, orbital parameters, topography, and sea ice and sea surface temperatures (SSTs) relevant to each time slice of interest. The final components are the BIOME4-trace gas (BIOME4-TG) equilibrium terrestrial biosphere model (Kaplan et al., 2006) and the Lund-Potsdam-Jena Lausanne-Mainz fire (LPJ-LMfire) dynamic global vegetation model (Pfeiffer et al., 2013). BIOME4-TG is used to determine static vegetation distributions, while LPJ-LMfire simulates biomass burning regimes. Meteorology from ModelE drives both these models, and the resulting land-cover characteristics and dry matter burned are implemented into GEOS-Chem. The offline-coupling approach of ICECAP allows sensitivity experiments to be performed relatively quickly. Also, by performing simulations in a stepwise manner, the chain of cause and effect can be readily diagnosed. A detailed description of the ICECAP model framework and its evaluation can be found in Murray et al. (2014).

As in Murray et al. (2014), we perform simulations for four different climate scenarios: present day (ca. 1990s); preindustrial (ca. 1770s); and two different representations of the LGM (~ 19–23 kyr) to span the range of likely conditions. The two LGM scenarios differ in the degree of cooling of tropical SSTs. Such differences have implications for LGM dynamics because of the influence of tropical SSTs on meridional temperature gradients and low-latitude circulation (Rind et al., 2009). The "warm LGM" uses the SST reconstructions from the Climate: long range Investigation, Mapping, and Prediction project (CLIMAP, 1976), with an average change in SST within 15° of the equator relative to the preindustrial ($\Delta SST_{15° S–° N}$) of −1.2 °C. The "cold LGM" uses SSTs from Webb et al. (1997) who found $\Delta SST_{15° S–° N}$ of −6.1 °C by imposing an ocean heat transport flux in an earlier version of the GISS climate model. A more recent estimate based on SST reconstructions from the MARGO project found $\Delta SST_{15° S–° N}$ of -1.7 ± 1.0 °C (Waelbroeck et al., 2009), which is more comparable to the warm LGM scenario used in this study.

ACPD
15, 2197–2246, 2015

Murray et al. (2014) also tested the sensitivity of their model results to uncertainties in lightning and fire emissions. Comparison with paleo-observations suggests that their "low-fire, variable-lightning, warm LGM" scenario was the best representation of the LGM atmosphere, in which lightning NO_x emissions are parameterized to reflect changes in convective cloud top heights, and the LPJ-LMfire fire emissions are scaled to match observational records inferred from the Global Charcoal Database (Power et al., 2007, 2010). The model simulations in this study are performed using the Murray et al. (2014) "best estimate" fire and lightning emission scenarios relevant for each climate.

2.2 Uncertainties in biogenic isoprene emissions

Biogenic VOC emissions in GEOS-Chem are calculated interactively by the Model of Emissions of Gases and Aerosols from Nature (MEGAN v2.1) (Guenther et al., 2012). The canopy-level flux of isoprene is computed as a function of plant function type (PFT)-specific basal emission rate, scaled by activity factors (γ_i) to account for environmental controlling factors including temperature, light availability, leaf age, and leaf area index (LAI). Tai et al. (2013) recently implemented an additional activity factor, γ_C, to account for the effect of atmospheric CO_2 concentrations. They used the empirical relationship from Possell and Hewitt (2011): $\gamma_C = a/(1 + abC)$, where the fitting parameters a and b have values of 8.9406 and 0.0024 ppm^{-1}, respectively, and C represents the atmospheric CO_2 concentration ($\gamma_C = 1$ at $C = 370$ ppm). To date, Possell and Hewitt (2011) studied the widest range of plant taxa and atmospheric CO_2 concentrations. Their CO_2-isoprene emission response curve shows a higher sensitivity at sub-ambient CO_2 concentrations than others from similar studies (e.g., Wilkinson et al., 2009), likely providing an upper limit of this effect for past climates.

Table 1 summarizes the prescribed CO_2 mixing ratios and the estimated total annual isoprene burdens with and without consideration of the CO_2-sensitivity of plant isoprene emissions for each climate scenario. Using the Possell and Hewitt (2011) relationship, we find increases in the total biogenic isoprene source of 28 % for the

ACPD
15, 2197–2246, 2015

preindustrial, 78 % for the warm LGM, and 77 % for the cold LGM scenarios, relative to estimates that do not take into account the CO_2-sensitivity.

Previous studies, which employ different global biogenic VOC emission models and land cover products to the ones used in this study, find that biogenic VOC emissions were 20–26 % higher in the preindustrial relative to the present day (Pacifico et al., 2012; Unger, 2013). In this study, we estimate this value to be 8 % when the CO_2-sensitivity of plant isoprene emissions is not considered, and 25 % when the CO_2-sensitivity is considered.

2.3 Uncertainties in the fate of the oxidation products of isoprene

2.3.1 Isoprene photo-oxidation mechanism

Murray et al. (2014) used the original GEOS-Chem isoprene photo-oxidation mechanism which is largely based on Horowitz et al. (1998). Here we apply recent updates to the mechanism by Mao et al. (2013c) and Paulot et al. (2009a, b). Daytime oxidation of isoprene by OH leads to the formation of hydroxyl-peroxy radicals ($ISOPO_2$). The new scheme includes a more explicit treatment of the production and subsequent reactions of organic nitrates, acids, and epoxides from reactions of the $ISOPO_2$ radicals. Such reactions lead to greater HO_x- and NO_x-regeneration and recycling than in the original mechanism, especially under low-NO_x conditions, which is of particular relevance for past atmospheres (Mao et al., 2013c). Beyond Mao et al. (2013c), we also change the stoichiometry of the ($ISOPO_2 + HO_2$) reaction to that recommended by the laboratory study of Liu et al. (2013), which has smaller uncertainties and leads to relatively smaller yields (by ~ 50 %) of HO_x, methyl vinyl ketone (MVK), and methacrolein (MACR) from this pathway. Our work tests the sensitivity of model results to these updates in the isoprene photo-oxidation mechanism.

ACPD
15, 2197–2246, 2015

2.3.2 Heterogeneous HO_2 uptake by aerosols

As parameterized in the standard GEOS-Chem model, gaseous HO_2 uptake by aqueous aerosols leads to H_2O_2 formation and has a $\gamma(HO_2)$ value typically less than 0.1, where $\gamma(HO_2)$ is a measure of the efficacy of uptake, defined as the fraction of HO_2 collisions with aerosol surfaces resulting in reaction. (Note that γ traditionally refers to both the aerosol uptake efficiency and biogenic emissions flux activity factor.) Atmospheric observations, however, suggest that HO_2 uptake by aerosols may in fact not produce H_2O_2 (de Reus et al., 2005; Mao et al., 2010). In light of these findings, Mao et al. (2013a) implemented a new uptake scheme in GEOS-Chem, in which HO_2 uptake yields H_2O via coupling of Cu(I) / Cu(II) and Fe(II) / Fe(III) ions, and we follow that approach here. As in Mao et al. (2013a), we use the upper limit of $\gamma(HO_2) = 1.0$ for all aerosol types to evaluate the implications of this uptake for the HO_x budgets and for the fate of the oxidation products of isoprene.

2.4 Outline of model sensitivity experiments

Table 2 summarizes the different climate, chemistry and plant isoprene emission scenarios tested in this model study. For each climate scenario, we apply to GEOS-Chem the archived meteorology and land cover products from the "best estimate" fire and lightning emission scenarios from Murray et al. (2014). We test three different chemistry schemes in GEOS-Chem: C1 uses the original isoprene chemistry and original HO_2 uptake; C2 uses the new isoprene chemistry and original HO_2 uptake; and C3 uses the new isoprene chemistry and new HO_2 uptake mechanisms. Each chemistry scheme is tested either with (w) or without (wo) inclusion of the CO_2-sensitivity of biogenic isoprene emissions, except for the present day. As Table 1 shows, consideration of the CO_2-sensitivity for the present day results in only a 4 % change in the global isoprene burden ($\gamma_C = 1$ at $C = 370$ ppm), and so we assume that the present-day model simulations with consideration of the CO_2-sensitivity of biogenic isoprene emissions are representative of their respective "without" scenarios. Our "C1-wo" model simula-

ACPD
15, 2197–2246, 2015

tions match the isoprene emissions and photochemistry schemes used by Murray et al. (2014) in their "best estimate" scenarios. We perform 21 simulations in total.

Each GEOS-Chem simulation is initialized over 10 years, repeatedly using the first year of archived meteorology, to reach equilibrium with respect to stratosphere-troposphere exchange. We then perform 3 more years of simulations for analysis.

3 Results

3.1 Tropospheric mean oxidant burdens

Figure 2 shows the simulated tropospheric mean mass-weighted burdens of OH, ozone, H_2O_2, and NO_3 for each combination of climate, chemistry and plant isoprene emission scenarios. The dotted orange line represents results using the "best estimate" lightning and fire emission scenarios of Murray et al. (2014). The plots show the varying sensitivity of oxidant levels to assumptions about the tropospheric chemical mechanism and the global isoprene burden.

Consideration of the CO_2-sensitivity of plant isoprene emissions yields larger isoprene emissions for the preindustrial and LGM scenarios (Table 1). For a given chemistry scheme and climate scenario, this leads to a decrease in the tropospheric mean OH burden, an increase in H_2O_2, and small changes in ozone and NO_3. This result can be understood by considering the classical tropospheric ozone-HO_x-NO_x-CO catalytic cycle (e.g., Rohrer et al., 2014, Fig. 1). In general, daytime oxidation of VOC by reaction with OH leads to formation of oxidized organic products and HO_2. Efficient HO_x-cycling depends on the presence of NO_x. Since low-NO_x conditions prevail in past atmospheres, an increased isoprene burden represents a net OH sink but an HO_2 source. The self-reaction of HO_2 leads to H_2O_2formation. Under low-NO_x conditions, tropospheric ozone production is relatively insensitive to changes in the reactive carbon burden. The tropospheric NO_3 burden also shows little change since the abundances of its precursors ($NO_2 + O_3$) hardly vary with the global isoprene burden.

ACPD
15, 2197–2246, 2015

Implementation of the new isoprene oxidation mechanism leads to large changes in tropospheric oxidant burdens of OH, O_3, and NO_3, but not H_2O_2, for the present and past atmospheres. Uncertainties in the isoprene mechanism are the largest source of uncertainties in global mean OH. Increases in the tropospheric mean OH burdens result from greater HO_x-regeneration in the new isoprene photo-oxidation cascade (Mao et al., 2013c). The ozone production efficiency – the number of ozone molecules produced per molecule of NO_x consumed (Liu et al., 1987) – is greater in the new isoprene mechanism, leading to increases in the tropospheric ozone burdens. This is because the newly added reactions of recycling of isoprene nitrates, formed in the ($ISOPO_2$+NO) reaction pathway, can lead to NO_x-regeneration, thereby representing a less permanent NO_x sink than nitric acid (Paulot et al., 2012). The present-day burden of NO_3 shows a large decrease in response to the new isoprene oxidation scheme, while those of the past atmospheres show little change. The muted NO_3 response for the past atmospheres is due to two competing effects in the new scheme: (1) an increased aerosol reactive uptake coefficient of NO_3 radicals (from 10^{-4} to 0.1) leading to greater NO_3 depletion (Mao et al., 2013c); and (2) increased abundances in both NO_3 precursors (NO_2+ O_3) enhancing its formation. The latter effect is due to greater NO_x-recycling and regeneration in the new scheme through isoprene nitrate recycling, and hence greater ozone production efficiency and increased lifetime of NO_x reservoir species. For the present-day, the increased abundances of NO_3 precursors are smaller than those of the past atmospheres. Finally, implementation of the new scheme of HO_2 uptake by aerosols leads to significant decreases in the tropospheric mean OH and H_2O_2 burdens in all simulations. This is due to both the higher efficacy of uptake than previously assumed and the formation of H_2O, instead of H_2O_2, as a by-product of the uptake, yielding a more efficient HO_x removal pathway.

Despite uncertainties in the isoprene emissions and photochemistry, we find reduced levels of ozone, H_2O_2, and NO_3 in each combination of chemistry and isoprene emission scenarios for the past atmospheres relative to the present-day, a result consistent with Murray et al. (2014). However, their conclusion that OH is relatively well buffered

ACPD
15, 2197–2246, 2015

on glacial-interglacial timescales relative to other tropospheric oxidants does not hold for some of the uncertainties explored in this study. Figure 3 shows the simulated percent changes in the tropospheric mean OH burden for the present-day, warm LGM, and cold LGM scenarios, relative to their respective preindustrial scenarios. Consideration of the CO_2-sensitivity of plant isoprene emissions alone (C1-w) leads to 23 and 29 % reductions in the tropospheric mean OH burden in the warm and cold LGM scenarios, relative to that of the preindustrial, while the present-day burden is 17 % greater than that of the preindustrial. When the new chemistry schemes are applied without consideration of the CO_2-sensitivity, the modeled changes in OH relative to the preindustrial are less dramatic but have opposite signs to those calculated under the C1-w scenarios for the present day and warm LGM. When all effects are considered (C2-w and C3-w), changes in the tropospheric mean OH burden across the warm LGM-to-preindustrial and preindustrial-to-present day transitions do not exceed 5 %, a result consistent with Murray et al. (2014). The varying sensitivity of the tropospheric mean OH burden to assumptions about the isoprene photochemistry and emissions has implications for our understanding of past methane and SOA burdens and radiative forcing calculations, as discussed in Sects. 3.3–3.4.

3.2 Comparison with observations

We evaluate the results of the model sensitivity experiments against four different categories of observations. Table 3 compares the simulated methyl chloroform (CH_3CCl_3) and methane lifetimes against loss from tropospheric OH under different chemistry schemes with observations for the present day. The global lifetimes of methyl chloroform and of methane against oxidation by tropospheric OH is calculated as the global burden divided by the total loss rate summed over all grid boxes in the troposphere:

ACPD
15, 2197–2246, 2015

$$\tau_{X,\mathrm{OH}} = \frac{\int_{\text{surface}}^{\text{TOA}} [X]\,\mathrm{d}x\,\mathrm{d}y\,\mathrm{d}z}{\int_{\text{surface}}^{\text{tropopause}} k_{\mathrm{X+OH}}(T)[\mathrm{OH}][X]\,\mathrm{d}x\,\mathrm{d}y\,\mathrm{d}z}, \quad (1)$$

where X represents either methyl chloroform or methane, and $k_{X+\mathrm{OH}}(T)$ is the temperature-dependent rate constant of the reaction. We assume that the mixing ratio of methyl chloroform is uniform throughout the troposphere and is 92 % lower than the total atmospheric concentration (Bey et al., 2001; Prather et al., 2012). For methane, the global burden is calculated from the mean surface concentration – prescribed as 1743 ppbv for the present day – using a conversion factor of 2.75 Tg CH_4 ppbv^{-1} from Prather et al. (2012). The combination of new isoprene and original HO_2 uptake chemistry (C2) has the largest simulated tropospheric mean OH burden (Fig. 2) and so yields the shortest methyl chloroform and methane lifetimes: 4.1 and 8.9 years, respectively. Prinn et al. (2005) inferred a methyl chloroform lifetime of $6.0^{+0.5}_{-0.4}$ years from observations of methyl chloroform and knowledge of its emissions. Our model results are all lower than this range, but comparable to recent multi-model estimates of 5.7 ± 0.9 years (Naik et al., 2013). Based on observations and emission estimates, Prinn et al. (2005) derived a mean methane lifetime of $10.2^{+0.9}_{-0.7}$ years between 1978–2004, and Prather et al. (2012) derived a methane lifetime of 11.2 ± 1.3 years for 2010. Although only the C1 value falls within this range, the slightly lower values given by the C2 and C3 chemistry schemes are still within the range of estimates reported by recent multi-model studies: 10.2 ± 1.7 years (Fiore et al., 2009), 9.8 ± 1.6 years (Voulgarakis et al., 2013) and 9.7 ± 1.5 years (Naik et al., 2013). Reconciling the magnitude of the inferred OH burden with modeled results remains an ongoing challenge (Holmes et al., 2013).

We also assess our model results for present-day OH by evaluating the simulated inter-hemispheric ratios (N / S) of tropospheric mean OH. Estimates of this ratio based on methyl chloroform measurements from 1980–2000 range between 0.85–

ACPD
15, 2197–2246, 2015

0.98, whereas the recent ACCMIP multi-model study finds a mean ratio of 1.28 ± 0.10 for 2000 (Naik et al., 2013; and references therein). For the years 2004–2011, Patra et al. (2014) finds an estimate of 0.97 ± 0.12 by optimizing model results to fit methyl chloroform measurements. In our present-day sensitivity experiments, we find a ratio of 1.20 for C1, 1.11 for C2, and 1.07 for C3. The models participating in the ACCMIP study did not consider HO_x-recycling pathways through reactions of peroxy and HO_2 radicals (Naik et al., 2013). As previously described, HO_x-recycling in the absence of NO_x can occur in our new isoprene photochemistry scheme (C2), which leads to a lower present-day N / S ratio of tropospheric mean OH. The decrease in this ratio is amplified when the upper limit of efficacy of HO_2 uptake by aerosols is considered (C3), because of large anthropogenic aerosol loadings in the Northern Hemisphere.

Figure 4 shows a comparison of CO surface concentrations over Antarctica between observations and our model results for the preindustrial and present-day simulations. CO influences the oxidative capacity of the troposphere through reaction with its primary sink, OH, which can subsequently affect the ozone budget (Fiore et al., 2012). In this context, CO can thus be a useful tool for evaluating the ability of chemistry transport models to simulate the tropospheric oxidative capacity (Haan and Raynaud, 1998). CO has a tropospheric lifetime of ~2 months (Novelli et al., 1998), and CO surface concentrations over Antarctica are thus influenced by oxidation processes throughout much of the Southern Hemisphere (Haan and Raynaud, 1998; van der Werf et al., 2013) . The NOAA Global Monitoring Division measured a mean CO surface concentration of 49 ± 2 ppbv for the 1990s, which is matched by all of our present-day simulations tested with different chemistry schemes. Wang et al. (2010) recently provided a 650-year Antarctic ice-core record of concentration and isotopic ratios of atmospheric CO. They measured CO surface concentrations at the South Pole of 48 ± 4 ppbv for the year 1777 (±110 years). Only one (C1-w) out of the six preindustrial simulations tested with different chemistry and isoprene emission schemes falls within the range of the observed value. However, in situ production of CO from organic substrates trapped

ACPD
15, 2197–2246, 2015

within the ice may complicate the comparison between ice-core CO and model results (Faïn et al., 2014; Guzmán et al., 2007; Haan and Raynaud, 1998).

Oxidants transfer unique isotopic signatures to the oxidation products, and we can take advantage of these signatures in our model evaluation if they are preserved in the ice-core record. The $\Delta^{17}O$ ($= \delta^{17}O - 0.52 \times \delta^{18}O$) of sulfate, known as $\Delta^{17}O(SO_4^{2-})$, and of nitrate, $\Delta^{17}O(NO_3^-)$, measure the departure from mass-dependent fractionation in its oxygen isotopes and reflect the relative importance of different oxidants in their atmospheric production pathways (Savarino et al., 2000). Sulfate formation primarily involves ozone, H_2O_2, and OH, while the main oxidants relevant to nitrate formation are ozone, RO_2 (R = H atom or organic group), OH, and BrO (Sofen et al., 2014). Such oxygen triple-isotope measurements have been used to infer the atmospheric formation pathways of sulfate and nitrate in the present from atmospheric sulfate and nitrate (e.g. Lee et al., 2001; Michalski, 2003), and in the past from ice-core sulfate and nitrate (e.g., Alexander et al., 2002, 2004). The dominant source region for Antarctic sulfate is the Southern Ocean marine boundary layer (MBL) (Sofen et al., 2011), while that for Antarctic nitrate is extra-tropical South America (Lee et al., 2014). We thus qualitatively compare our model results for these respective regions with Antarctic ice-core measurements of $\Delta^{17}O(SO_4^{2-})$ and $\Delta^{17}O(NO_3^-)$.

Measurements of $\Delta^{17}O(SO_4^{2-})$ from the WAIS Divide ice core imply that the $[O_3]/[OH]$ ratio in the Southern ocean MBL may have increased by 260 % since the early 19th century, while measurements of $\Delta^{17}O(NO_3^-)$ suggest that the $[O_3]/[RO_2]$ ratio in the Southern Hemisphere extratropical troposphere may have decreased by 60–90 % between the 1860s and 2000, assuming no change (≤ 5 %) in OH (Sofen et al., 2014). Table 4 lists the simulated percent changes in surface $[O_3]/[OH]$ and $[O_3]/[RO_2]$ in the present day scenarios relative to their respective preindustrial scenarios. For $[O_3]/[OH]$, the signs of change are all consistent with the ice-core measurements, but our model greatly underestimates the values inferred from observations, with values ranging from 3 to 42 %. Our model also underestimates the changes in $[O_3]/[RO_2]$ compared to observations. Our modeled increase (5–10 %) in OH abun-

ACPD
15, 2197–2246, 2015

dance in the extra-tropical South American boundary layer in the present day would further lower $\Delta^{17}O(NO_3^-)$, which is qualitatively consistent with the observations. However, accounting for both modeled decreases in $[O_3]/[RO_2]$ and [OH] still underestimates the observed decrease in $\Delta^{17}O(NO_3^-)$ by 75–85 %. These mismatches may be due to deficiencies in our current understanding and model representation of remote marine boundary layer sulfate formation and of nitrate formation, as suggested by Sofen et al. (2014). On glacial-interglacial timescales, measurements of $\Delta^{17}O(SO_4^{2-})$ from the Vostok ice core imply that gas-phase oxidation by OH contributed up to 40 % more to sulfate production during the last glacial period relative to the interglacial periods before and after (Alexander et al., 2002). Here our simulated percent changes in surface OH concentrations over the Southern Ocean between the LGM and preindustrial scenarios are more comparable to the observations, with values ranging from 68 to 120 % for the warm LGM and 87 to 117 % for the cold LGM scenarios (Table 4). Ongoing measurements of the $\Delta^{17}O$ in ice-core sulfate and nitrate over the last glacial-interglacial cycle will allow for further model evaluation. Measurements of $\Delta^{17}O(NO_3^-)$ may in fact be a more robust proxy than those of $\Delta^{17}O(SO_4^{2-})$ for reconstructing the oxidation capacity of past atmospheres because of its greater sensitivity to oxidant abundances. For example, cloud amount and pH do not influence the isotopic composition of nitrate as they do for sulfate (Levine et al., 2011).

3.3 Implications for the methane budget

The global methane lifetime against oxidation by tropospheric OH, $\tau_{CH_4,OH}$, is calculated as defined by Eq. (1). In GEOS-Chem, atmospheric methane concentrations are prescribed from observations – the tropospheric mean concentrations are 1743 ppbv for the present day, 731 ppbv for the preindustrial, and 377 ppbv for the LGM scenarios (Murray et al., 2014, Table 3). The approximately doubled methane concentration across the LGM-to-preindustrial transition implies a decrease in methane emissions or in its lifetime against oxidation, or some combination of both factors, at the LGM.

ACPD
15, 2197–2246, 2015

The left panels of Fig. 5 show the global methane lifetimes against oxidation by tropospheric OH for each combination of climate, chemistry, and isoprene emission scenarios. The dotted orange line represents results using the "best estimate" lightning and fire emission scenarios of Murray et al. (2014). Consideration of the CO_2-sensitivity of plant isoprene emissions alone leads to large increases in the past global isoprene emissions, which in turn depress the tropospheric mean OH burden, thereby lengthening the methane lifetimes by 1.2 years for the preindustrial, 5.4 years for the warm LGM, and 5.8 years for the cold LGM. Conversely, implementation of the new isoprene photooxidation scheme leads to larger OH burdens, resulting in decreases in the methane lifetimes – by 1.4 years for the present day, 2.6 years for the preindustrial, 3.2 years for the warm LGM, and 4.0 years for the cold LGM. Implementation of the new HO_2 uptake scheme dampens the OH burden, which in turn slightly increases the methane lifetimes for each climate scenario.

We compare the sensitivity of the changes in the global methane lifetimes and in the implied emissions relative to the preindustrial in the right panels of Fig. 5. Results from the "best estimate" scenarios of Murray et al. (2014) suggest that relative to the preindustrial, the global methane lifetime is reduced by 0.7 years in the present, and is increased by 0.4 years at the LGM. This minimal increase in the lifetime at the LGM puts a higher burden on sources in explaining the glacial-interglacial variability of atmospheric methane concentration. Assuming no large changes occurred in the minor loss mechanisms, methane emissions scale with changes in its loss by OH in the troposphere. As defined in Sect. 3.2, the total loss rate of methane with respect to OH oxidation in the troposphere ($\mathrm{Tg\,yr^{-1}}$) is calculated from the integral: $\int_{\text{surface}}^{\text{tropopause}} k_{CH_4+OH}(T)[OH][CH_4]\,dx\,dy\,dz$. For their "best estimate" scenarios, Murray et al. (2014) reports that total methane emissions are 150 % higher in the present relative to the preindustrial and are reduced by 50 % at the LGM. In our study, consideration of the CO_2-sensitivity of plant isoprene emissions alone shortens the methane lifetime by 1.9 years in the present relative to the preindustrial, and lengthens it by 4.6 years

ACPD
15, 2197–2246, 2015

at the LGM. This result suggests that methane emissions are reduced by 63 % at the LGM relative to the preindustrial, which places an even larger burden on sources than in Murray et al. (2014) in explaining the glacial-interglacial variability of atmospheric methane concentration. On the other hand, implementation of the new isoprene photo-
5 oxidation scheme, either with or without consideration of the CO_2-sensitivity of plant isoprene emissions, results in relatively small changes in methane lifetimes across the glacial-interglacial or preindustrial-to-present day timescales. The resulting estimates of the reductions in methane emissions at the LGM relative to the preindustrial (between 46–52 %) are consistent with the Murray et al. (2014) finding.

10 In summary, the calculated change in global methane lifetime at the LGM relative to the preindustrial ranges between −0.4 to +4.6 years across our ensemble of sensitivity simulations. This range implies a reduction in methane emissions greater than or comparable to the estimated value of 50 % by Murray et al. (2014) in their "best estimate" scenario. Our estimates are also greater than the 29–42 % decrease in wetland emis-
15 sions simulated by the PMIP2 ensemble members (Weber et al., 2010), and the 16 and 23 % decreases in natural methane emissions simulated by Kaplan et al. (2006) and Valdes (2005), respectively.

3.4 Implications for SOA burdens and radiative forcing

Isoprene oxidation products substantially contribute to SOA formation (Henze and Se-
20 infeld, 2006), and so our results have implications for trends in SOA burden and radiative forcing. Increasingly cooler global temperatures relative to the present day in the preindustrial, warm LGM, and cold LGM scenarios are expected to decrease biogenic isoprene emissions. However, such reductions are dampened or offset when the sensitivity to atmospheric CO_2 is also considered, since biogenic isoprene emissions
25 are enhanced at CO_2 concentrations below present-day levels. The left panel of Fig. 6 shows the global SOA burdens for each combination of climate, chemistry, and isoprene emission scenarios. The dotted orange line represents results using the "best estimate" lightning and fire emission scenarios of Murray et al. (2014). Consideration

ACPD
15, 2197–2246, 2015

of the CO_2-sensitivity of plant isoprene emissions alone leads to large increases in the past global isoprene burdens, which subsequently increases SOA at the preindustrial and LGM. For example, under the C1 chemistry scheme, the relative increases in the SOA burden are 24 % for the preindustrial, 93 % for the warm LGM, and 80 % for the cold LGM scenario when the CO_2-sensitivity of plant isoprene emissions is considered compared to the cases when it is not. Conversely, for a given isoprene emission scenario, changes to the isoprene photo-oxidation and HO_2 uptake schemes lead to much smaller changes in the SOA burdens in each climate scenario.

The right panel of Fig. 6 shows the percent changes in tropospheric mean SOA burdens relative to their respective preindustrial scenarios. The "best estimate" scenarios of Murray et al. (2014) – represented by our "C1-wo" simulations – suggest that relative to the preindustrial, the total SOA burden is 5 % lower in the present, 42 % lower at the warm LGM, and 50 % lower at the cold LGM. These values, while relatively robust to variations in the isoprene photo-oxidation and HO_2 uptake schemes, are sensitive to estimates of the global isoprene burdens for the past atmospheres; consideration of the CO_2-sensitivity of plant isoprene emissions enhances the present-to-preindustrial difference but reduces the LGM-to-preindustrial differences in the global SOA burden. For example, under the C1 chemistry scheme, consideration of the CO_2-sensitivity of plant isoprene emissions leads to decreases of 23 % in the total SOA burden in the present, but only of 10 and 28 % in the warm and cold LGM scenarios, relative to the preindustrial.

3.5 Factors controlling variability in the tropospheric oxidative capacity

Murray et al. (2014) identified the key parameters that appear to control global mean OH levels on glacial-interglacial timescales. In this section, we explore the robustness of their result to the uncertainties in isoprene photochemistry and emissions tested in this study. Using the steady-state equations of the ozone-NO_x-HO_x-CO system, Wang and Jacob (1998) derived a linear relationship between the global mean OH burden and

ACPD
15, 2197–2246, 2015

the ratio $S_N / \left(S_C^{3/2}\right)$, where S_N and S_C are the tropospheric sources of reactive nitrogen (Tmol N yr^{-1}) and of reactive carbon (Tmol C yr^{-1}), respectively. Murray et al. (2014) found that on glacial-interglacial timescales, the linear relationship can be maintained if two additional factors, which Wang and Jacob (1998) had assumed constant in their derivation, are also considered: (1) the mean tropospheric ozone photolysis frequency, J_{O_3} (s^{-1}) and (2) the tropospheric water vapor concentration, represented by the specific humidity, q (g H_2O kg air^{-1}). In other words,

$$[OH] \propto J_{O_3} q S_N / \left(S_C^{3/2}\right) \quad (2)$$

Figure 7 shows a plot of the tropospheric mean OH burden for each simulation as a function of $J_{O_3} q S_N / \left(S_C^{3/2}\right)$, divided into panels according to the chemistry scheme. As in Murray et al. (2014), S_C is calculated as the sum of emissions of CO and NMVOCs and an implied source of methane equal to its loss rate by OH. While Murray et al. (2014) assumed that each molecule of isoprene yields an average 2.5 carbons that go on to react in the gas phase, this assumption has been found to not be robust for different isoprene oxidation schemes, and so we assume that each isoprene molecule undergoes 100 % gas-phase oxidation for all of the three chemistry schemes tested in this study.

Only the C1 data subset shows a statistically significant correlation coefficient; a reduced major axis regression fit is shown by the orange line (Fig. 7). The breakdown in linearity for the C2 and C3 subsets can by explained by examining the classical tropospheric NO_x-HO_x-CO-ozone chemistry, upon which the linear relationship is derived. In this classical chemistry system, HO_x-cycling is coupled to NO_x-cycling. However, the new isoprene photo-oxidation mechanism includes additional pathways for HO_x-regeneration and recycling in the absence of NO_x. The new mechanism thus permits HO_x-cycling to occur without subsequent production of ozone through NO_2 photolysis, thereby weakening the sensitivity of OH to each of the individual components of

ACPD
15, 2197–2246, 2015

$J_{O_3} q S_N / \left(S_C^{3/2}\right)$. For example, Murray et al. (2014) found that the global mean OH independently varied weakly but most strongly with the photolysis component (J_{O_3}) in their simulations. In this study, the only subset of simulations exhibiting a statistically significant correlation between OH and J_{O_3} is C1-wo ($R^2 = 0.99$, $n = 4$). This scheme employs the original isoprene and HO_2 uptake schemes without consideration of the CO_2-sensitivity of plant isoprene emissions – i.e., the same as that used by Murray et al. (2014).

In Fig. 7, it can be seen that the slopes of the relationship appear to change between the LGM-to-preindustrial and preindustrial-to-present day transitions for all of the three data subsets. We test whether the slope and intercept values are significantly different between the chemistry schemes by fitting a multiple regression model with $J_{O_3} q S_N / \left(S_C^{3/2}\right)$ as a continuous explanatory variable and chemistry scheme as a categorical explanatory variable. We find that the three correlations have different values for the intercepts whereas the values for the slopes do not significantly differ (Fig. 7, dashed grey lines). The value of the intercept is largest for the C2 ensemble, followed by C3, and then C1, indicating that mean OH is sensitive to the chemistry scheme used. This sequence follows from our finding that the new isoprene photooxidation mechanism leads to larger tropospheric mean OH burdens for each climate scenario compared to those simulated by the original mechanism. Implementation of the new HO_2 uptake scheme dampens this increase, but values remain above those from the C1 ensemble (Sect. 3.1). We postulate two main reasons why the slope of OH to $J_{O_3} q S_N / \left(S_C^{3/2}\right)$ appears to be lower across the industrial era than across the glacial-interglacial period. First, it is likely that heterogeneous reactions that can also act as HO_x sinks but are not considered in the derivation of the linear relationship, such as N_2O_5 hydrolysis and HO_2 uptake by aerosols, become more important under present-day conditions. In the present day, tropospheric aerosol mass loading is 17–20 % higher than the preindustrial, and 36–52 % higher than the warm and cold LGM scenarios. Second, there is a dramatic shift in the altitudinal distribution of tropo-

ACPD
15, 2197–2246, 2015

spheric NO_x emissions. The ratio of lightning to surface NO_x emissions is 0.16 for the present day, 0.50 for the preindustrial, 0.73 for the warm LGM, and 0.79 for the cold LGM. The much lower present-day ratio is primarily due to large anthropogenic surface NO_x emissions, especially in the Northern Hemisphere (Murray et al., 2014, Fig. 5). This could lead to relatively more efficient NO_x removal by wet and dry deposition, and by formation of organic nitrates, which would both reduce primary and secondary OH production. However, these hypotheses need to be examined in greater detail, and an evaluation of potential weaknesses of the linear relationship between OH and $J_{O_3} q S_N / \left(S_C^{3/2}\right)$ that operate independently of the classic photo-oxidation mechanism is described by Murray et al. (2015).

4 Discussion and conclusions

Using a detailed climate-biosphere-chemistry framework, we evaluate the sensitivity of modeled tropospheric oxidant levels to recent advances in our understanding of biogenic isoprene emissions and of the fate of isoprene oxidation products in the atmosphere. We focus on this sensitivity for the present day (ca. 1990s), preindustrial (ca. 1770s), and the Last Glacial Maximum (LGM, ~19–23 kyr). The 3-D global ICECAP model employed here considers the full suite of key factors controlling the oxidative capacity of the troposphere, including the effect of changes in the stratospheric column ozone on tropospheric photolysis rates (Murray et al., 2014). Our study, which revisits Murray et al. (2014), takes into account the sensitivity of plant isoprene emissions to atmospheric CO_2 levels, and considers the effects of a new isoprene photo-oxidation (Paulot et al., 2009a, b) and a potentially larger role for heterogeneous HO_2 uptake Mao et al., 2013a). To our knowledge, this is the first model study to perform a systematic evaluation of the sensitivity of the chemical composition of past atmospheres to these developments.

ACPD
15, 2197–2246, 2015

We simulate two possible realizations of the LGM, one significantly colder than the other, to bound the range of uncertainty in the extent of tropical cooling at the LGM. For each climate scenario, we test three different chemistry schemes: C1, the original isoprene chemistry and original HO_2 uptake; C2, the new isoprene chemistry and original HO_2 uptake; and C3, the new isoprene chemistry and new HO_2 uptake mechanisms. Each chemistry scheme is tested with or without inclusion of the CO_2-sensitivity of biogenic isoprene emissions, except for the present day for which consideration of the CO_2-sensitivity results in only a 4 % change in the global isoprene burden. We find that consideration of the CO_2-sensitivity of biogenic emissions enhances plant isoprene emissions by 27 % in the preindustrial and by 77–78 % at the LGM, relative to respective estimates that do not take into account the CO_2-sensitivity.

We find that different oxidants have varying sensitivity to the assumptions tested in this study, with OH being the most sensitive. Although Murray et al. (2014) estimated that OH is relatively well buffered on glacial-interglacial timescales, we find that this result is not robust to all of the assumptions tested in this study, especially with respect to uncertainties in the isoprene photo-oxidation mechanism. Changes in the global mean OH levels for the LGM-to-preindustrial transition range between −29 and +7 %, and those for the preindustrial-to-present day transition range between −8 and +17 %, across our sensitivity simulations. However, consistent with Murray et al. (2014), we find reduced levels of ozone, H_2O_2, and NO_3 for the past atmospheres relative to the present-day in our ensemble of sensitivity simulations. That study also reported a linear relationship between OH and tropospheric mean ozone photolysis rates, water vapor, and total emissions of NO_x and reactive carbon ($J_{O_3} q S_N / \left(S_C^{3/2}\right)$) on LGM-to-present day timescales. We find that the new isoprene photo-oxidation mechanism causes a breakdown in this linear relationship across the entire period, as the new mechanism permits HO_x-cycling to occur without subsequent production of ozone through NO_2 photolysis, thereby weakening the feedback on OH production per RO_2 consumed. We propose that the sensitivity of OH to changes in $J_{O_3} q S_N / \left(S_C^{3/2}\right)$ may be lower for the

ACPD
15, 2197–2246, 2015

preindustrial-to-present day than the LGM-to-preindustrial transition. This is most likely because NO_x and HO_x loss processes not considered in the classical NO_x-HO_x-CO-ozone system (from which the linear relationship is derived) become more important under present-day conditions. All of our sensitivity experiments are broadly consistent with ice-core records of $\Delta^{17}O$ of sulfate and nitrate at the LGM and of CO in the preindustrial. For the present-day, the C1 chemistry scheme shows the best agreement with observation-based estimates of methane and methyl chloroform lifetimes, whereas C3 shows the best agreement with observation-based estimates of the inter-hemispheric (N / S) ratio of tropospheric mean OH. Thus, it is challenging to identify the most likely chemistry and isoprene emission scenarios.

We find that the calculated change in global methane lifetime at the LGM relative to the preindustrial ranges between −0.4 to +4.6 years across our ensemble of sensitivity simulations. This range implies a reduction in methane emissions greater than or comparable to the best estimate value of 50 % by Murray et al. (2014), which corroborates their finding that the observed glacial-interglacial variability in atmospheric methane is predominantly driven by changes in its sources as opposed to its sink with OH. Our findings also have implications for radiative forcing estimates of SOA on preindustrial-present and glacial-interglacial timescales. For example, the "best estimate" scenarios of Murray et al. (2014) suggest that relative to the preindustrial, the total SOA burden is 5 % lower in the present and 42 % lower at the LGM. Here, we find decreases ranging between 2–23 % in the present and 10–44 % at the LGM relative to the preindustrial across our sensitivity experiments. The climate effects of biogenic SOA are not well characterized, but are thought to provide regional cooling (Scott et al., 2014). Our work thus suggests that SOA reductions may have amplified regional warming in the present but minimized regional cooling at the LGM, relative to the preindustrial. Results from the sensitivity studies, however, underscore the large uncertainties in current model estimates of SOA radiative forcing across long time scales (e.g., Scott et al., 2014; Unger and Yue, 2014; Unger, 2014).

ACPD
15, 2197–2246, 2015

Unger (2014) recently quantified the radiative forcing from global cropland expansion between the 1850s and 2000s, with a focus on changes in biogenic VOC emissions, which influence preindustrial-to-present day changes in ozone, methane, and biogenic SOA burdens. She found a net cooling of $-0.11 \pm 0.17\,\mathrm{W\,m^{-2}}$ due to changing biogenic VOC emissions from global land use changes, which is comparable in magnitude but opposite in sign to the net forcing from the changes in surface albedo and land carbon release associated with cropland expansion. Our work demonstrates that besides changes in land use, changes in environmental factors controlling biogenic VOC emissions should also be included in calculations of the net radiative forcing. For example, Unger (2014) reported a decrease in biogenic VOC emissions of 37 % due to expanding cropland, but did not include the effects of meteorological variables or CO_2-sensitivity on such emissions. In our study, biogenic VOC emissions decrease by just 8 % in the present day relative to the preindustrial due to changing meteorology and land use change, and by 25 % when the CO_2-sensitivity of isoprene emissions is also considered.

The primary goal of this model study is to explore the sensitivity of the oxidative capacity of present and past atmospheres to assumptions about isoprene emissions and the fate of its oxidation products. We do not attempt to offer "best guess" estimates for the following reasons. First, the parameterization of the CO_2-isoprene interaction used in this study is based on a limited number of plant taxa (Possell and Hewitt, 2011), and differs substantially from another proposed form of the response curve at sub-ambient CO_2 levels (Wilkinson et al., 2009). Models of biogenic VOC emissions, such as the one employed in this study, remain uncertain as they rely on a limited number of measurements (Barkley et al., 2011). Until we have a better understanding of why plants emit isoprene, uncertainties in estimates of past and future biogenic isoprene emissions will likely persist (Pacifico et al., 2009). Second, knowledge of the photochemical cascade of isoprene oxidation is still evolving. Updated mechanisms are still unable to fully reconcile measured and modeled OH concentrations (Mao et al., 2012). The reactivity of isoprene nitrates, which could significantly affect the efficiency of ozone

ACPD
15, 2197–2246, 2015

production, is not well understood (e.g., Lee et al., 2014; Müller et al., 2014). Rohrer et al. (2014) reported a linear dependence of OH on local ozone photolysis rates at two sites with vastly different NO_x concentrations in China, a result at odds with our current understanding of the theoretical dependence of OH on NO_x. Third, considerable uncertainties still exist in mechanisms of SOA formation from VOC precursors (Henze and Seinfeld, 2006). Formation of SOA in the GEOS-Chem CTM is predicted based upon rate constants and aerosol yield parameters determined from laboratory chamber studies, which may not be representative of atmospheric conditions (Karambelas et al., 2014). We also do not consider cloud processing of isoprene oxidation products and condensation onto inorganic aerosol species, which could increase the predicted SOA yields from isoprene oxidation (Liao et al., 2007). Such processes are beyond the scope of this study but warrants further investigation. Lastly, the limited availability of direct observations of past oxidant levels hinders our ability to quantitatively assess results from our model sensitivity experiments.

This study highlights the importance of biogenic VOC emissions and the fate of their oxidation products in influencing chemistry-climate interactions across the last glacial-interglacial time interval and the industrial era. The range of uncertainties in our results demonstrates how current understanding of isoprene emissions and photochemistry remains inadequate, thereby impeding our ability to constrain the oxidative capacities of the present and past atmospheres, its controlling factors, and the radiative forcing of trends in short-lived species such as SOA over time. All of our present-day sensitivity experiments underestimate methane and methyl chloroform lifetimes inferred from observations. Our findings corroborate those of the recent Atmospheric Chemistry and Climate Model Intercomparison Project that uncertainties in our understanding of the long-term trends in OH and methane lifetime will persist unless natural precursor emissions and chemical mechanisms are well constrained (Naik et al., 2013). In addition, our results call for greater attention and research efforts in improving model representations of SOA formation from VOC precursors and heterogeneous reactions that act as HO_x and NO_x sinks – such processes may influence the present-day sensitivity of

ACPD
15, 2197–2246, 2015

OH to NO_x emissions. We recommend that as knowledge of the environmental factors controlling biogenic isoprene emissions and of the isoprene photo-oxidation mechanism evolves, re-evaluating model estimates of the oxidative capacities of past atmospheres should be a priority for future research. In particular, our ability to reconcile the discrepancies between measured and modeled HO_x concentrations in regions with low-NO_x and high-VOC concentrations will be of particular importance for improving model estimates of the oxidative capacities of present and past atmospheres.

Author contributions. P. Achakulwisut and L. J. Mickley designed the experiments and P. Achakulwisut performed the model simulations and analysis. L. T. Murray, A. P. K. Tai, and J. O. Kaplan developed the model code. P. Achakulwisut prepared the manuscript with contributions for all co-authors.

Acknowledgements. The authors would like to thank Mirjam Pfeiffer for performing the LPJ-LMfire simulations, John Mak for providing ice-core CO data, and Daniel Jacob, Karena McKinney, Fabien Paulot, and Malcolm Possell for stimulating discussions. This project was funded by NSF grant AGS-1102880 to Harvard University and to the University of Washington.

References

Alexander, B., Savarino, J., Barkov, N. I., Delmas, R. J., and Thiemens, M. H.: Climate driven changes in the oxidation pathways of atmospheric sulfur, Geophys. Res. Lett., 29, 30-1–30-4, doi:10.1029/2002GL014879, 2002.

Alexander, B., Savarino, J., Kreutz, K. J., and Thiemens, M. H.: Impact of preindustrial biomass-burning emissions on the oxidation pathways of tropospheric sulfur and nitrogen, J. Geophys. Res., 109, D08303, doi:10.1029/2003JD004218, 2004.

Barkley, M. P., Palmer, P. I., Ganzeveld, L., Arneth, A., Hagberg, D., Karl, T., and Yantosca, R. M.: Can a "state of the art" chemistry transport model simulate Amazonian tropospheric chemistry?, J. Geophys. Res., 116, D16302, doi:10.1029/2011JD015893, 2011.

Beerling, D. J., Nicholas Hewitt, C., Pyle, J. A., and Raven, J. A.: Critical issues in trace gas biogeochemistry and global change, Philosophical Transactions Series A, Mathematical, Physical, and Engineering Sciences, 365, 1629–1642, doi:10.1098/rsta.2007.2037, 2007.

ACPD
15, 2197–2246, 2015

Bey, I., Jacob, D. J., Yantosca, R. M., Logan, J. A., Field, B. D., Fiore, A. M., and Schultz, M. G.: Global modeling of tropospheric chemistry with assimilated meteorology: Model description and evaluation, J. Geophys. Res., 106, 23073, doi:10.1029/2001JD000807, 2001.

Brook, E. J., Harder, S., Severinghaus, J., Steig, E. J., and Sucher, C. M.: On the origin and timing of rapid changes in atmospheric methane during the last glacial period, Global. Biogeochem. Cy., 14, 559–572, 2000.

CLIMAP: The Surface of the Ice-Age Earth, Science (New York, N.Y.), 191, 1131–1137, 1976.

de Reus, M., Fischer, H., Sander, R., Gros, V., Kormann, R., Salisbury, G., Van Dingenen, R., Williams, J., Zöllner, M., and Lelieveld, J.: Observations and model calculations of trace gas scavenging in a dense Saharan dust plume during MINATROC, Atmos. Chem. Phys., 5, 1787–1803, doi:10.5194/acp-5-1787-2005, 2005.

Faïn, X., Chappellaz, J., Rhodes, R. H., Stowasser, C., Blunier, T., McConnell, J. R., Brook, E. J., Preunkert, S., Legrand, M., Debois, T., and Romanini, D.: High resolution measurements of carbon monoxide along a late Holocene Greenland ice core: evidence for in situ production, Clim. Past., 10, 987–1000, doi:10.5194/cp-10-987-2014, 2014.

Fiore, A. M., Dentener, F. J., Wild, O., Cuvelier, C., Schultz, M. G., Hess, P., and Zuber, A.: Multimodel estimates of intercontinental source-receptor relationships for ozone pollution, J. Geophys. Res., 114, D04301, doi:10.1029/2008JD010816, 2009.

Fiore, A. M., Naik, V., Spracklen, D. V, Steiner, A., Unger, N., Prather, M., and Zeng, G.: Global air quality and climate, Chem. Soc. Rev., 41, 6663–6683, doi:10.1039/c2cs35095e, 2012.

Guenther, A. B., Jiang, X., Heald, C. L., Sakulyanontvittaya, T., Duhl, T., Emmons, L. K., and Wang, X.: The Model of Emissions of Gases and Aerosols from Nature version 2.1 (MEGAN2.1): an extended and updated framework for modeling biogenic emissions, Geosci. Model. Dev., 5, 1471–1492, doi:10.5194/gmd-5-1471-2012, 2012.

Guenther, A., Karl, T., Harley, P., Wiedinmyer, C., Palmer, P. I., and Geron, C.: Estimates of global terrestrial isoprene emissions using MEGAN (Model of Emissions of Gases and Aerosols from Nature), Atmos. Chem. Phys., 6, 3181–3210, doi:10.5194/acp-6-3181-2006, 2006.

Guzmán, M. I., Hoffmann, M. R., and Colussi, A. J.: Photolysis of pyruvic acid in ice: Possible relevance to CO and CO_2 ice core record anomalies, J. Geophys. Res., 112, D10123, doi:10.1029/2006JD007886, 2007.

ACPD
15, 2197–2246, 2015

Haan, D., and Raynaud, D.: Ice core record of CO variations during the last two millennia: atmospheric implications and chemical interactions within the Greenland ice, Tellus, 50B, 253–262, 1998.

Harder, S. L., Shindell, D. T., Schmidt, G. A., and Brook, E. J.: A global climate model study of CH4 emissions during the Holocene and glacial-interglacial transitions constrained by ice core data, Global. Biogeochem. Cy., 21, GB1011, doi:10.1029/2005GB002680, 2007.

Henze, D. K. and Seinfeld, J. H.: Global secondary organic aerosol from isoprene oxidation, Geophys. Res. Lett., 33, L09812, doi:10.1029/2006GL025976,2006.

Hewitt, C. N., Lee, J. D., MacKenzie, A. R., Barkley, M. P., Carslaw, N., Carver, G. D., Chappell, N. A., Coe, H., Collier, C., Commane, R., Davies, F., Davison, B., DiCarlo, P., Di Marco, C. F., Dorsey, J. R., Edwards, P. M., Evans, M. J., Fowler, D., Furneaux, K. L., Gallagher, M., Guenther, A., Heard, D. E., Helfter, C., Hopkins, J., Ingham, T., Irwin, M., Jones, C., Karunaharan, A., Langford, B., Lewis, A. C., Lim, S. F., MacDonald, S. M., Mahajan, A. S., Malpass, S., McFiggans, G., Mills, G., Misztal, P., Moller, S., Monks, P. S., Nemitz, E., Nicolas-Perea, V., Oetjen, H., Oram, D. E., Palmer, P. I., Phillips, G. J., Pike, R., Plane, J. M. C., Pugh, T., Pyle, J. A., Reeves, C. E., Robinson, N. H., Stewart, D., Stone, D., Whalley, L. K., and Yin, X.: Overview: oxidant and particle photochemical processes above a south-east Asian tropical rainforest (the OP3 project): introduction, rationale, location characteristics and tools, Atmos. Chem. Phys., 10, 169–199, doi:10.5194/acp-10-169-2010, 2010.

Hofzumahaus, A., Rohrer, F., Lu, K., Bohn, B., Brauers, T., Chang, C.-C., and Zhang, Y.: Amplified trace gas removal in the troposphere, Science (New York, N.Y.), 324, 1702–1704, doi:10.1126/science.1164566, 2009.

Holmes, C. D., Prather, M. J., Søvde, O. A., and Myhre, G.: Future methane, hydroxyl, and their uncertainties: key climate and emission parameters for future predictions, Atmos. Chem. Phys., 13, 285–302, doi:10.5194/acp-13-285-2013, 2013.

Horowitz, L. W., Liang, J., Gardner, G. M., and Jacob, D. J.: Export of reactive nitrogen from North America during summertime: Sensitivity to hydrocarbon chemistry, J. Geophys. Res., 103, 13451–13476, 1998.

Hutterli, M. A., Bales, R. C., Mcconnell, J. R., and Stewart, R. W.: HCHO in Antarctic snow: Preservation in ice cores and air-snow exchange, Geophys. Res. Lett., 29, 1235, doi:10.1029/2001GL014256, 2002.

Isaksen, I. S. and Dalsøren, S. B.: Atmospheric science. Getting a better estimate of an atmospheric radical, Science (New York, N.Y.), 331, 38–39, doi:10.1126/science.1199773, 2011.

ACPD
15, 2197–2246, 2015

Khalil, M. A. K. and Rasmussen, R. A.: Atmospheric methane: Trends over the last 10 000 years, Atmos. Environ., 21, 2445–2452, 1987.
Kaplan, J. O.: Wetlands at the Last Glacial Maximum: Distribution and methane emissions, Geophys. Res. Lett., 29, 1079, doi:10.1029/2001GL013366, 2002.
Kaplan, J. O., Folberth, G., and Hauglustaine, D. A.: Role of methane and biogenic volatile organic compound sources in late glacial and Holocene fluctuations of atmospheric methane concentrations, Global Biogeochem. Cy., 20, GB2016, doi:10.1029/2005GB002590, 2006.
Karambelas, A., Pye, H. O. T., Budisulistiorini, S. H., Surratt, J. D., and Pinder, R. W.: Contribution of Isoprene Epoxydiol to Urban Organic Aerosol: Evidence from Modeling and Measurements, Environ. Sci. Technol. Lett., 1, 278–283, doi:10.1021/ez5001353, 2014.
Lathière, J., Hauglustaine, D. A., De Noblet-Ducoudré, N., Krinner, G., and Folberth, G. A.: Past and future changes in biogenic volatile organic compound emissions simulated with a global dynamic vegetation model, Geophys. Res. Lett., 32, L20818, doi:10.1029/2005GL024164, 2005.
Lee, H.-M., Henze, D. K., Alexander, B., and Murray, L. T.: Investigating the sensitivity of surface-level nitrate seasonality in Antarctica to primary sources using a global model, Atmos. Environ., 89, 757–767, doi:10.1016/j.atmosenv.2014.03.003, 2014.
Lee, L., Teng, A. P., Wennberg, P. O., Crounse, J. D., and Cohen, R. C.: On Rates and Mechanisms of OH and O3 Reactions with Isoprene-Derived Hydroxy Nitrates, J. Phys. Chem-A., 118, 1622–1637, 2014.
Lee, C. C. W.,Savarino, J., and Thiemsen, M. H.: Mass independent oxygen isotopic composition of atmospheric sulfate: Origin and implications for the present and past atmospheres of Earth and Mars, Geophys. Res. Lett., 28, 1783–1786, 2001.
LeGrande, A. N., Schmidt, G. A., Shindell, D. T., Field, C. V, Miller, R. L., Koch, D. M., and Hoffmann, G.: Consistent simulations of multiple proxy responses to an abrupt climate change event, P. Natl. Acad. Sci. USA, 103, 837–842, 2006.
Lelieveld, J., Butler, T. M., Crowley, J. N., Dillon, T. J., Fischer, H., Ganzeveld, L., and Williams, J.: Atmospheric oxidation capacity sustained by a tropical forest, Nature, 452, 737–740, doi:10.1038/nature06870, 2008.
Levine, J. G., Wolff, E. W., Jones, A. E., Hutterli, M. A., Wild, O., Carver, G. D., and Pyle, J. A.: In search of an ice core signal to differentiate between source-driven and sink-driven changes in atmospheric methane, J. Geophys. Res., 116, D05305, doi:10.1029/2010JD014878, 2011.

ACPD
15, 2197–2246, 2015

Liao, H., Henze, D. K., Seinfeld, J. H., Wu, S., and Mickley, L. J.: Biogenic secondary organic aerosol over the United States?: Comparison of climatological simulations with observations, J. Geophys. Res., 112, 1–19, doi:10.1029/2006JD007813, 2007.
Liu, S. C., Trainer, M., Fehsenfeld, F. C., Parrish, D. D., Williams, E. J., Fahey, D. W., and Murphy, P. C.: Ozone production in the rural troposphere and the implications for regional and global ozone distributions, J. Geophys. Res., 92, 4191–4207, 1987.
Liu, Y. J., Herdlinger-Blatt, I., McKinney, K. A., and Martin, S. T.: Production of methyl vinyl ketone and methacrolein via the hydroperoxyl pathway of isoprene oxidation, Atmos. Chem. Phys., 13, 5715–5730, doi:10.5194/acp-13-5715-2013, 2013.
Mao, J., Fan, S., Jacob, D. J., and Travis, K. R.: Radical loss in the atmosphere from Cu-Fe redox coupling in aerosols, Atmos. Chem. Phys., 13, 509–519, doi:10.5194/acp-13-509-2013, 2013.
Mao, J., Jacob, D. J., Evans, M. J., Olson, J. R., Ren, X., Brune, W. H., Clair, J. M. St., Crounse, J. D., Spencer, K. M., Beaver, M. R., Wennberg, P. O., Cubison, M. J., Jimenez, J. L., Fried, A., Weibring, P., Walega, J. G., Hall, S. R., Weinheimer, A. J., Cohen, R. C., Chen, G., Crawford, J. H., McNaughton, C., Clarke, A. D., Jaeglé, L., Fisher, J. A., Yantosca, R. M., Le Sager, P., and Carouge, C.: Chemistry of hydrogen oxide radicals (HO_x) in the Arctic troposphere in spring, Atmos. Chem. Phys., 10, 5823–5838, doi:10.5194/acp-10-5823-2010, 2010.
Mao, J., Paulot, F., Jacob, D. J., Cohen, R. C., Crounse, J. D., Wennberg, P. O., and Horowitz, L. W.: Ozone and organic nitrates over the eastern United States: Sensitivity to isoprene chemistry, J. Geophys. Res.-Atmos., 118, 11256–11268, doi:10.1002/jgrd.50817, 2013.
Mao, J., Ren, X., Zhang, L., Van Duin, D. M., Cohen, R. C., Park, J.-H., Goldstein, A. H., Paulot, F., Beaver, M. R., Crounse, J. D., Wennberg, P. O., DiGangi, J. P., Henry, S. B., Keutsch, F. N., Park, C., Schade, G. W., Wolfe, G. M., Thornton, J. A., and Brune, W. H.: Insights into hydroxyl measurements and atmospheric oxidation in a California forest, Atmos. Chem. Phys., 12, 8009–8020, doi:10.5194/acp-12-8009-2012, 2012.
Michalski, G.: First measurements and modeling of Δ 17 O in atmospheric nitrate, Geophys. Res. Lett., 30, 1870, doi:10.1029/2003GL017015, 2003.
McLinden, C. A., Olsen, S. C., Hannegan, B. ., Wild, O., and Prather, M. J.: Stratospheric ozone in 3D models: A simple chemistry and the cross-tropopause flux, J. Geophys. Res., 14653–14665, 2000.
Müller, J.-F., Peeters, J., and Stavrakou, T.: Fast photolysis of carbonyl nitrates from isoprene, Atmos. Chem. Phys., 14, 2497–2508, doi:10.5194/acp-14-2497-2014, 2014.

ACPD
15, 2197–2246, 2015

Murray, L. T., Mickley, L. J., Kaplan, J. O., Sofen, E. D., Pfeiffer, M., and Alexander, B.: Factors controlling variability in the oxidative capacity of the troposphere since the Last Glacial Maximum, Atmos. Chem. Phys., 14, 3589–3622, doi:10.5194/acp-14-3589-2014, 2014.

Murray, L. T., Fiore, A. M., Shindell, D. T., Naik, V., Horowitz, L. W., and Evans, M. J.: Uncertainties in global atmospheric hydroxyl projections tied to fate of reactive nitrogen and carbon, in preparation, 2015.

Naik, V., Voulgarakis, A., Fiore, A. M., Horowitz, L. W., Lamarque, J.-F., Lin, M., Prather, M. J., Young, P. J., Bergmann, D., Cameron-Smith, P. J., Cionni, I., Collins, W. J., Dalsøren, S. B., Doherty, R., Eyring, V., Faluvegi, G., Folberth, G. A., Josse, B., Lee, Y. H., MacKenzie, I. A., Nagashima, T., van Noije, T. P. C., Plummer, D. A., Righi, M., Rumbold, S. T., Skeie, R., Shindell, D. T., Stevenson, D. S., Strode, S., Sudo, K., Szopa, S., and Zeng, G.: Preindustrial to present-day changes in tropospheric hydroxyl radical and methane lifetime from the Atmospheric Chemistry and Climate Model Intercomparison Project (ACCMIP), Atmos. Chem. Phys., 13, 5277–5298, doi:10.5194/acp-13-5277-2013, 2013.

Novelli, P. C., Masarie, K. A., and Lang, P. M.: Distributions and recent changes of carbon monoxide in the lower troposphere, J. Geophys. Res., 103, 19015–19033, doi:10.1029/98JD01366, 1998.

Pacifico, F., Folberth, G. A., Jones, C. D., Harrison, S. P., and Collins, W. J. Sensitivity of biogenic isoprene emissions to past, present, and future environmental conditions and implications for atmospheric chemistry, J. Geophys. Res.-Atmos., 117, D22303, doi:10.1029/2012JD018276, 2012.

Pacifico, F., Harrison, S. P., Jones, C. D., and Sitch, S.: Isoprene emissions and climate, Atmos. Environ., 43, 6121–6135, doi:10.1016/j.atmosenv.2009.09.002, 2009.

Park, R. J.: Natural and transboundary pollution influences on sulfate-nitrate-ammonium aerosols in the United States: Implications for policy, J. Geophys. Res., 109, D15204, doi:10.1029/2003JD004473, 2004.

Parrella, J. P., Jacob, D. J., Liang, Q., Zhang, Y., Mickley, L. J., Miller, B., Evans, M. J., Yang, X., Pyle, J. A., Theys, N., and Van Roozendael, M.: Tropospheric bromine chemistry: implications for present and pre-industrial ozone and mercury, Atmos. Chem. Phys., 12, 6723–6740, doi:10.5194/acp-12-6723-2012, 2012.

Patra, P. K., Krol, M. C., Montzka, S. a, Arnold, T., Atlas, E. L., Lintner, B. R., and Young, D.: Observational evidence for interhemispheric hydroxyl-radical parity, Nature., 513, 219–223, doi:10.1038/nature13721, 2014.

ACPD
15, 2197–2246, 2015

Paulot, F., Crounse, J. D., Kjaergaard, H. G., Kroll, J. H., Seinfeld, J. H., and Wennberg, P. O.: Isoprene photooxidation: new insights into the production of acids and organic nitrates, Atmos. Chem. Phys., 9, 1479–1501, doi:10.5194/acp-9-1479-2009, 2009.

Paulot, F., Crounse, J. D., Kjaergaard, H. G., Kürten, A., Clair, J. M. S., Seinfeld, J. H., and Wennberg, P. O.: Unexpected Epoxide Formation in the Gas-Phase Photooxidation of Isoprene, Science (New York, N.Y.), 325, 730–733, 2009.

Paulot, F., Henze, D. K., and Wennberg, P. O.: Impact of the isoprene photochemical cascade on tropical ozone, Atmos. Chem. Phys., 12, 1307–1325, doi:10.5194/acp-12-1307-2012, 2012.

Paulot, F., Jacob, D. J., and Henze, D. K.: Sources and Processes Contributing to Nitrogen Deposition: An Adjoint Model Analysis Applied to Biodiversity Hotspots Worldwide, Environ. Sci. Technol., 47, 3226–3233, 2013.

Pavelin, E. G., Johnson, C. E., Rughooputh, S., and Toumi, R.: Evaluation of pre-industrial surface ozone measurements made using Schönbein's method, Atmos. Environ., 33, 919–929, 1999.

Pfeiffer, M., Spessa, A., and Kaplan, J. O.: A model for global biomass burning in preindustrial time: LPJ-LMfire (v1.0), Geosci. Model Dev., 6, 643–685, doi:10.5194/gmd-6-643-2013, 2013.

Pike, R. C. and Young, P. J.: How plants can influence tropospheric chemistry?: the role of isoprene emissions from the biosphere, Weather, 64, 332–336, 2009.

Possell, M. and Hewitt, C. N.: Isoprene emissions from plants are mediated by atmospheric CO_2 concentrations, Glob. Change. Biol., 17, 1595–1610, doi:10.1111/j.1365-2486.2010.02306.x, 2011.

Power, M. J., Marlon, J., Ortiz, N., Bartlein, P. J., Harrison, S. P., Mayle, F. E., and Zhang, J. H.: Changes in fire regimes since the Last Glacial Maximum: an assessment based on a global synthesis and analysis of charcoal data, Clim. Dynam., 30, 887–907, doi:10.1007/s00382-007-0334-x, 2007.

Power, M. J., Marlon, J. R., Bartlein, P. J., and Harrison, S. P.: Fire history and the Global Charcoal Database: A new tool for hypothesis testing and data exploration, Palaeogeogr. Palaeocl., 291, 52–59, doi:10.1016/j.palaeo.2009.09.014, 2010.

Prather, M. J., Holmes, C. D., and Hsu, J.: Reactive greenhouse gas scenarios: Systematic exploration of uncertainties and the role of atmospheric chemistry, Geophys. Res. Lett., 39, L09803, doi:10.1029/2012GL051440, 2012.

ACPD
15, 2197–2246, 2015

Prinn, R. G., Huang, J., Weiss, R. F., Cunnold, D. M., Fraser, P. J., Simmonds, P. G., and Krummel, P. B.: Evidence for variability of atmospheric hydroxyl radicals over the past quarter century, Geophys. Res. Lett., 32, L07809, doi:10.1029/2004GL022228, 2005.

Rind, D., Chandler, M., Lonergan, P., and Lerner, J.: Climate change and the middle atmosphere: 5. Paleostratosphere in cold and warm climates, J. Geophys. Res., 106, 20195, doi:10.1029/2000JD900548, 2001.

Rind, D., Lerner, J., McLinden, C., and Perlwitz, J.: Stratospheric ozone during the Last Glacial Maximum, Geophys. Res. Lett., 36, L09712, doi:10.1029/2009GL037617, 2009.

Rohrer, F., Lu, K., Hofzumahaus, A., Bohn, B., Brauers, T., Chang, C.-C., and Wahner, A.: Maximum efficiency in the hydroxyl-radical-based self-cleansing of the troposphere, Nat. Geosci., 7, 559–563, doi:10.1038/ngeo2199, 2014.

Savarino, J., Lee, C. C. W., and Thiemens, M. H.: Laboratory oxygen isotopic study of sulfur(IV) oxidation: Origin of the mass-independent oxygen isotopic anomaly in atmospheric sulfates and sulfate mineral deposits on Earth, J. Geophys. Res., 105, 29079–29088, 2000.

Scott, C. E., Rap, A., Spracklen, D. V., Forster, P. M., Carslaw, K. S., Mann, G. W., Pringle, K. J., Kivekäs, N., Kulmala, M., Lihavainen, H., and Tunved, P.: The direct and indirect radiative effects of biogenic secondary organic aerosol, Atmos. Chem. Phys., 14, 447–470, doi:10.5194/acp-14-447-2014, 2014.

Sitch, S., Cox, P. M., Collins, W. J., and Huntingford, C.: Indirect radiative forcing of climate change through ozone effects on the land-carbon sink, Nature, 448, 791–794, doi:10.1038/nature06059, 2007.

Sofen, E. D., Alexander, B., and Kunasek, S. A.: The impact of anthropogenic emissions on atmospheric sulfate production pathways, oxidants, and ice core $\Delta^{17}O(SO_4^{2-})$, Atmos. Chem. Phys., 11, 3565–3578, doi:10.5194/acp-11-3565-2011, 2011.

Sofen, E. D., Alexander, B., Steig, E. J., Thiemens, M. H., Kunasek, S. A., Amos, H. M., Schauer, A. J., Hastings, M. G., Bautista, J., Jackson, T. L., Vogel, L. E., McConnell, J. R., Pasteris, D. R., and Saltzman, E. S.: WAIS Divide ice core suggests sustained changes in the atmospheric formation pathways of sulfate and nitrate since the 19th century in the extratropical Southern Hemisphere, Atmos. Chem. Phys., 14, 5749–5769, doi:10.5194/acp-14-5749-2014, 2014.

Tai, A. P. K., Mickley, L. J., Heald, C. L., and Wu, S.: Effect of CO2 inhibition on biogenic isoprene emission: Implications for air quality under 2000 to 2050 changes in climate, vegetation, and land use, Geophys. Res. Lett., 40, 3479–3483, doi:10.1002/grl.50650, 2013.

ACPD
15, 2197–2246, 2015

Thornton, J. A., Jaeglé, L. and McNeill, V. F.: Assessing known pathways for HO_2 loss in aqueous atmospheric aerosols: Regional and global impacts on tropospheric oxidants, J. Geophys. Res.-Atmos., 113, D05303, doi:10.1029/2007JD009236, 2008.

Trowbridge, A. M., Asensio, D., Eller, A. S. D., Way, D. A., Wilkinson, M. J., Schnitzler, J.-P., and Monson, R. K.: Contribution of various carbon sources toward isoprene biosynthesis in poplar leaves mediated by altered atmospheric CO2 concentrations, PloS One, 7, e32387, doi:10.1371/journal.pone.0032387, 2012.

Unger, N.: Isoprene emission variability through the twentieth century, J. Geophys. Res.-Atmos., 118, 13606–13613, doi:10.1002/2013JD020978, 2013.

Unger, N.: Human land-use-driven reduction of forest volatiles cools global climate, Nature Climate Change, 4, 1–4, doi:10.1038/nclimate2347, 2014.

Unger, N. and Yue, X.: Strong chemistry-climate feedbacks in the Pliocene, Geophys. Res. Lett., 41, 527–533, doi:10.1002/2013GL058773, 2014.

Valdes, P. J.: The ice age methane budget, Geophys. Res. Lett., 32, L02704, doi:10.1029/2004GL021004, 2005.

van der Werf, G. R., Peters, W., van Leeuwen, T. T., and Giglio, L.: What could have caused pre-industrial biomass burning emissions to exceed current rates?, Clim. Past., 9, 289–306, doi:10.5194/cp-9-289-2013, 2013.

van der Werf, G. R., Randerson, J. T., Giglio, L., Collatz, G. J., Mu, M., Kasibhatla, P. S., Morton, D. C., DeFries, R. S., Jin, Y., and van Leeuwen, T. T.: Global fire emissions and the contribution of deforestation, savanna, forest, agricultural, and peat fires (1997–2009), Atmos. Chem. Phys., 10, 11707–11735, doi:10.5194/acp-10-11707-2010, 2010.

Voulgarakis, A., Naik, V., Lamarque, J.-F., Shindell, D. T., Young, P. J., Prather, M. J., Wild, O., Field, R. D., Bergmann, D., Cameron-Smith, P., Cionni, I., Collins, W. J., Dalsøren, S. B., Doherty, R. M., Eyring, V., Faluvegi, G., Folberth, G. A., Horowitz, L. W., Josse, B., MacKenzie, I. A., Nagashima, T., Plummer, D. A., Righi, M., Rumbold, S. T., Stevenson, D. S., Strode, S. A., Sudo, K., Szopa, S., and Zeng, G.: Analysis of present day and future OH and methane lifetime in the ACCMIP simulations, Atmos. Chem. Phys., 13, 2563–2587, doi:10.5194/acp-13-2563-2013, 2013.

Waelbroeck, C., Paul, A., Kucera, M., Rosell-Melé, A., Weinelt, M., Schneider, R., and Turon, J.-L.: Constraints on the magnitude and patterns of ocean cooling at the Last Glacial Maximum, Nature Geosci., 2, 127–132, doi:10.1038/ngeo411, 2009.

ACPD
15, 2197–2246, 2015

Wang, Y. and Jacob, D. J.: Anthropogenic forcing on tropospheric ozone and OH since preindustrial times, J. Geophys. Res.-Atmos., 103, 31123–31135, doi:10.1029/1998JD100004, 1998.

Wang, Z., Chappellaz, J., Park, K., and Mak, J. E.: Large variations in Southern Hemisphere biomass burning during the last 650 years, Science (New York, N.Y.), 330, 1663–1666, doi:10.1126/science.1197257, 2010.

Webb, R. S., Rind, D. H., Lehman, S. J., Healy, R. J., and Sigman, D.: Influence of ocean heat transport on the climate of the Last Glacial Maximum, Nature, 385, 695–699, 1997.

Weber, S. L., Drury, A. J., Toonen, W. H. J., and van Weele, M.: Wetland methane emissions during the Last Glacial Maximum estimated from PMIP2 simulations: Climate, vegetation, and geographic controls, J. Geophys. Res., 115, D06111, doi:10.1029/2009JD012110, 2010.

Wilkinson, M. J., Monson, R. K., Trahan, N., Lee, S., Brown, E., Jackson, R. B., and Fall, R.: Leaf isoprene emission rate as a function of atmospheric CO2 concentration. Glob. Change. Biol., 15, 1189–1200, doi:10.1111/j.1365-2486.2008.01803.x, 2009.

ACPD
15, 2197–2246, 2015

Table 1. Atmospheric CO_2 concentrations and global annual terrestrial plant isoprene emissions for each climate scenario.

Climate Scenario	$[CO_2]$ (ppmv)	Global Annual Terrestrial Plant Isoprene Emissions		
		without CO_2-sensitivity ($Tg\,C\,yr^{-1}$)	with[a] CO_2-sensitivity ($Tg\,C\,yr^{-1}$)	Percent change with CO_2-sensitivity relative to without (%)
Present day	354	536	557	+3.9
Preindustrial	280	580	740	+28
Warm LGM	188	478	849	+78
Cold LGM	188	261	463	+77

[*] This study uses the empirical relationship from Possell and Hewitt (2011) to test the sensitivity of plant isoprene emissions to atmospheric CO_2 concentrations.

ACPD
15, 2197–2246, 2015

Table 2. Summary of the different climate, chemistry and plant isoprene emission scenarios tested in this model study. For each climate scenario except for the present day, all possible combinations of chemistry and emission schemes are tested (for the present day, only the "with" CO_2-sensitivity scheme is used). We perform 21 simulations in total.

Climate	Notes
Present day	ca. 1990s
Preindustrial	ca. 1770s
Warm LGM	19-23 ka; SSTs from CLIMAP Project Members(1967) with $\Delta SST^{a}_{15^\circ S-^\circ N}$ of −1.2 °C
Cold LGM	19–23 ka; SSTs from Webb et al. (1997) with $\Delta SST^{a}_{15^\circ S-^\circ N}$ of −6.1 °C
Chemistry	**Notes (color scheme used in figures)**
C1[b]	Original isoprene chemistry and original HO_2 uptake (orange)
C2	New isoprene chemistry and original HO_2 uptake (green)
C3	New isoprene chemistry and new HO_2 uptake (blue)
CO_2-sensitivity of plant isoprene emission	**Notes**
Without (wo)[b]	Controlling factors include temperature, light availability, leaf age, and leaf area index (LAI)
With (w)	Controlling factors include the above and atmospheric CO_2 concentrations

[a] The average change in sea surface temperature (SST) within 15 ° of the equator relative to the preindustrial.
[b] The "C1-wo" combination corresponds to the schemes used by Murray et al. (2014) in their "best estimate" scenarios.

ACPD
15, 2197–2246, 2015

Table 3. Calculated present-day methyl chloroform (MCF) and methane lifetimes against tropospheric oxidation by OH ($\tau_{MCF,OH}$, $\tau_{CH_4,OH}$), with consideration of CO_2-sensitivity of plant isoprene emissions.

	Model Chemistry Scheme[a]			
Lifetime	C1	C2	C3	Lifetimes inferred from observations
$\tau_{MCF,OH}$ [yr]	4.8	4.1	4.5	$6.0^{+0.5}_{-0.4}$[b]
$\tau_{CH_4,OH}$ [yr]	10.3	8.9	9.6	11.2 ± 1.3[c]

[a] See Table 2 for a full description of the different chemistry schemes tested in this study.
[b] Inferred from observations (Prinn et al., 2005).
[c] Inferred from observations (Prather et al., 2012).

ACPD
15, 2197–2246, 2015

Table 4. Modeled percent changes in the surface $[O_3]/[OH]$ and $[O_3]/[RO_2]$ ratios for the present day relative to the preindustrial, and in the surface [OH] concentration for the warm and cold LGM relative to the preindustrial, for different model sensitivity experiments. Surface $[O_3]/[OH]$ and [OH] values are averaged over the 46–66° S latitude band to compare with values inferred from ice-core measurements of $\Delta^{17}O(SO_4^{2-})$ by Sofen et al. (2014) and Alexanderet al. (2002). Surface $[O_3]/[RO_2]$ are averaged over the 34–54° S and 62.5–72.5° W (extratropical South America) to compare with values inferred from ice-core measurements of $\Delta^{17}O(NO_3^-)$ by Sofen et al. (2014), as described in Sect. 3.2.

Chemistry* Scheme	CO_2 -sensitivity of plant isoprene emissions	Present day – Preindustrial: Percent change in surface $[O_3]/[OH]$ over 46–66° S (%)	Present day – Preindustrial: Percent change in surface $[O_3]/[RO_2]$ over S. America (%)	Warm LGM – Preindustrial: Percent change in surface [OH] over 46–66° S (%)	fCold LGM – Preindustrial: Percent change in surface [OH] over 46–66° S (%)
C1	without	35	2.3	68	87
	with	39	−0.3	105	106
C2	without	42	5.1	93	95
	with	42	2.8	105	101
C3	without	38	2.5	102	109
	with	40	−0.4	120	117

* See Table 2 for a full description of the different chemistry schemes tested in this study.

ACPD
15, 2197–2246, 2015

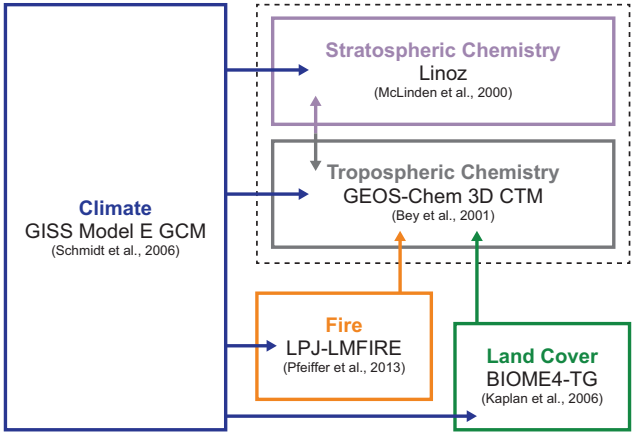

Figure 1. The ICE age Chemistry And Proxies (ICECAP) model framework consists of four global models, represented here by boxes with solid lines. The stratospheric and tropospheric chemistry schemes are coupled online in the GEOS-Chem Chemical Transport Model (CTM). Arrows indicate the flow of model output. The ICECAP model framework was especially designed for simulating the oxidative capacity of past atmospheres. (Adapted from Murray et al., 2014, Fig. 1.)

ACPD
15, 2197–2246, 2015

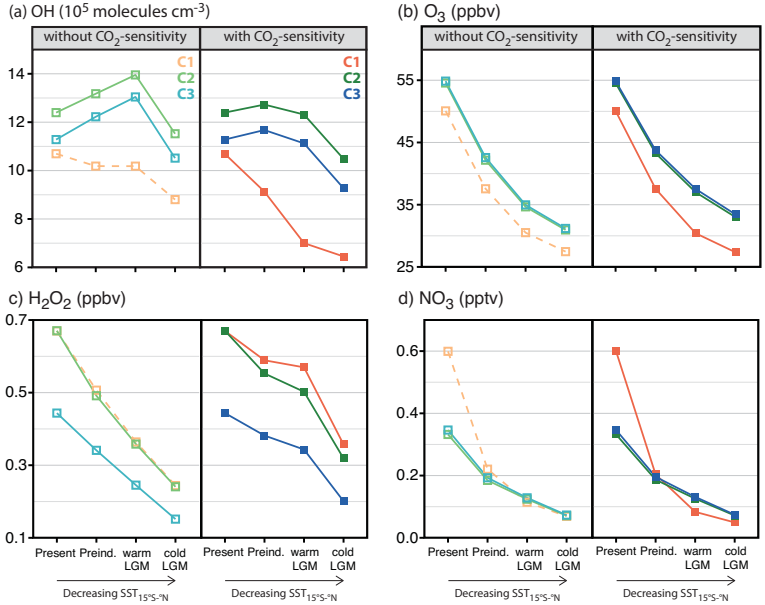

Figure 2. Simulated sensitivity of the tropospheric mean mass-weighted oxidant burdens of OH, O_3, H_2O_2, and NO_3 to each combination of climate, chemistry, and plant isoprene emission scheme. Simulations are as described in Table 2. The climate scenarios are present day, preindustrial, warm LGM, and cold LGM, with decreasing sea surface temperatures within 15° of the equator ($SST_{15°S-°N}$), going from left to right along the abscissa. The chemistry schemes are C1 (orange curves), C2 (green), and C3 (blue). Plant isoprene emissions are modeled without (light-shaded) or with (dark-shaded) sensitivity to atmospheric CO_2 concentrations. The tropospheric burdens are calculated with the tropopause determined from the thermal lapse rate. The dotted light-orange line represents the results reported in Murray et al. (2014) for their "best estimate" lightning and fire emissions scenarios.

ACPD
15, 2197–2246, 2015

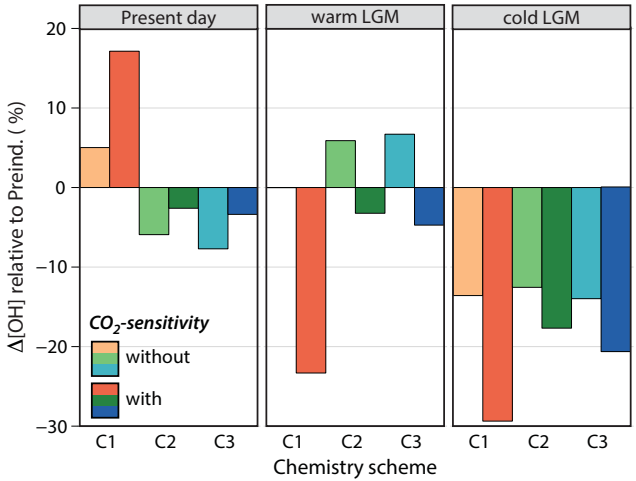

Figure 3. Percent changes (%) in the tropospheric mean mass-weighted OH burden for a range of scenarios relative to their respective preindustrial scenarios. Simulations are as described in Table 2. The climate scenarios are present day, preindustrial, warm LGM, and cold LGM. The chemistry schemes are C1 (orange bars), C2 (green), and C3 (blue). Plant isoprene emissions are modeled without (light-shaded) or with (dark-shaded) sensitivity to atmospheric CO_2 concentrations. For the present day, test simulations with and without CO_2-sensitivity yield nearly identical isoprene emissions. We therefore perform all present-day simulations with CO_2-sensitivity turned on and assume that these model results apply to the respective present-day "without" scenarios. (Note: The percent change at the warm LGM relative to the preindustrial is very small when the C1 chemistry scheme is used without consideration of the CO_2-sensitivity (C1-wo), and so no light orange bar is apparent in the middle panel.)

ACPD
15, 2197–2246, 2015

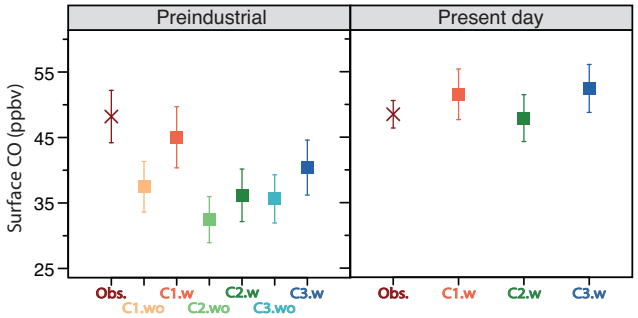

Figure 4. Comparison of model results with observations of CO surface concentrations (ppbv) over Antarctica for the preindustrial (1770s) and present-day (1990s) simulations. Simulations are as described in Table 2; colors are as in Fig. 2. The maroon crosses represent observations from different sources for each time slice. Wang et al. (2010) measured ice-core CO concentrations at the South Pole of 48 ± 4 ppbv for the year 1777 (±110 years); the associated errors represent analytical uncertainties. The mean CO surface concentration measured at the South Pole by the NOAA Global Monitoring Division for the 1990s is 49 ± 2 ppbv; the associated errors represent inter-annual variability. The squares represent values averaged over Antarctica from our model simulations tested with different chemistry and isoprene emission schemes for the preindustrial and present-day scenarios. Simulations are as described in Table 2; colors are as in Fig. 2. Error bars associated with the model results represent ±1 standard deviation of the spatially-averaged mean value.

ACPD
15, 2197–2246, 2015

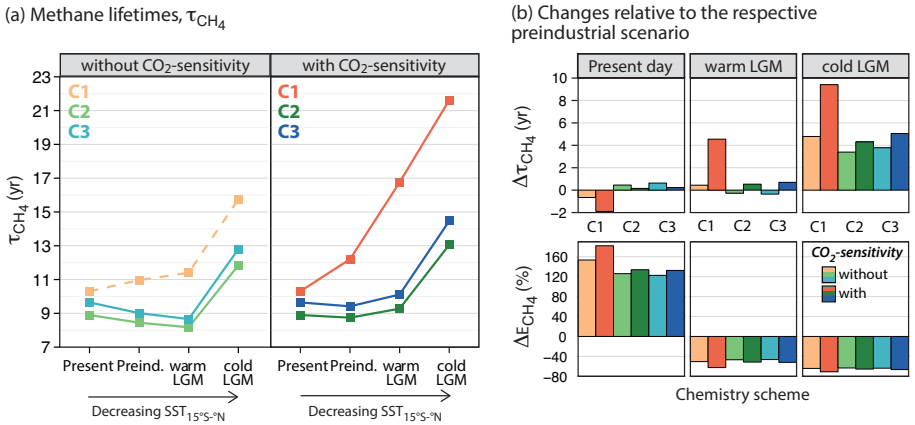

Figure 5. Left Panel: calculated global methane lifetime against oxidation by tropospheric OH for each combination of climate, chemistry and plant isoprene emission scenarios. Simulations are as described in Table 2; colors are as in Fig. 2. The dotted light-orange line represents the results reported in Murray et al. (2014) for their "best estimate" lightning and fire emissions scenarios. Right Panels: Changes in the global methane lifetimes (yr) and emissions (%) relative to their respective preindustrial scenarios. Colors are as in Fig. 3. Changes in methane emissions are calculated by assuming that they scale with changes in methane loss by OH in the troposphere.

ACPD
15, 2197–2246, 2015

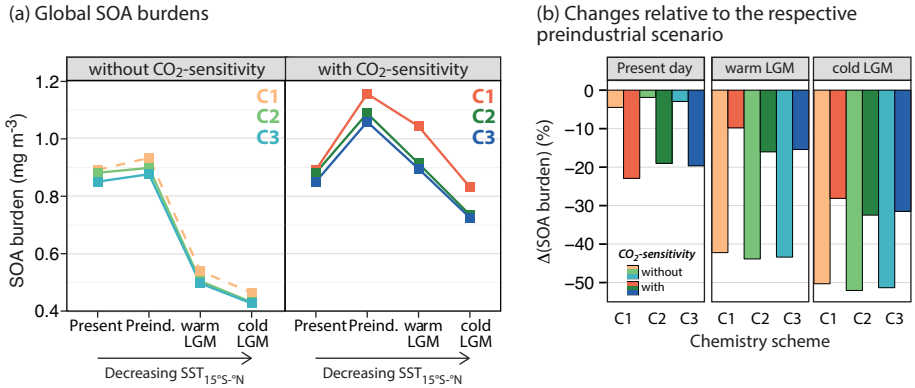

Figure 6. Left Panel: tropospheric mean mass-weighted secondary organic aerosol (SOA) burdens for each combination of climate, chemistry and plant isoprene emission scenarios. Simulations are as described in Table 2; colors are as in Fig. 2. The dotted light-orange line represents the results reported in Murray et al. (2014) for their "best estimate" lightning and fire emissions scenarios. Right Panel: Percent changes in tropospheric mean SOA burdens relative to their respective preindustrial scenarios. Colors are as in Fig. 3.

ACPD
15, 2197–2246, 2015

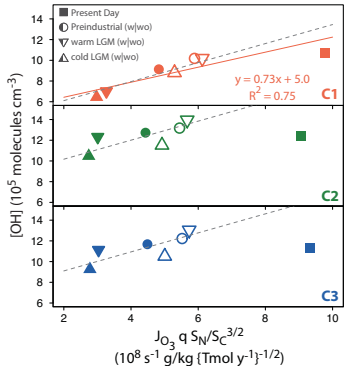

Figure 7. Tropospheric mean mass-weighted OH burden in each simulation as a function of $J_{O_3} q S_N / \left(S_C^{3/2}\right)$, where J_{O_3} is the tropospheric mean mass-weighted ozone photolysis frequency (s^{-1}), q is the tropospheric mean mass-weighted specific humidity ($g\,kg^{-1}$), and S_N and S_C are the tropospheric sources of reactive nitrogen ($Tmol\,N\,a^{-1}$) and of reactive carbon ($Tmol\,C\,a^{-1}$), respectively. S_C is calculated as the sum of emissions of CO, NMVOCs, and an implied source of methane equal to its loss rate by OH. Model results for different chemistry schemes are separated into three subsets as follows. Top panel: original isoprene chemistry and original HO_2 uptake (C1). Middle panel: new isoprene chemistry and original HO_2 uptake (C2). Bottom panel: new isoprene chemistry and new HO_2 uptake (C3). Different symbols denote different climate scenarios (present day, preindustrial, warm LGM, cold LGM). Filled symbols represent simulations in which the CO_2-sensitivity of plant isoprene emission is considered (w); unfilled symbols are those without (wo). All present-day simulations were performed with CO_2-sensitivity turned on. The orange line shows a reduced major axis regression fit for the C1 subset, with the regression equation and coefficient of determination (R^2) inset. We do not find a statistically significant correlation between OH and $J_{O_3} q S_N / \left(S_C^{3/2}\right)$ for the C2 and C3 subsets. When the present-day values are excluded and a multiple regression model is fitted to the remaining ensemble, we find that the three different chemistry schemes possess the same values for the slopes of the linear correlation but different values for the intercepts, as shown by the dashed grey lines (see text for details).

ACPD
15, 2197–2246, 2015